

Epigenetic silencing of callose synthase by VIL1 promotes bud-growth transition in lily bulbs

Received: 7 February 2023

Accepted: 12 July 2023

Published online: 10 August 2023

Wenqiang Pan  ^{1,8}, Jingru Li  ^{1,8}, Yunpeng Du  ^{2,8}, Yajie Zhao  ¹, Yin Xin  ¹, Shaokun Wang  ¹, Chang Liu  ¹, Zhimin Lin  ³, Shaozhong Fang  ³, Yingdong Yang ⁴, Michele Zaccai  ⁵, Xiuhai Zhang  ², Mingfang Yi  ¹, Sonia Gazzarrini  ^{6,7} & Jian Wu  ¹✉

 Check for updates

In plants, restoring intercellular communication is required for cell activity in buds during the growth transition from slow to fast growth after dormancy release. However, the epigenetic regulation of this phenomenon is far from understood. Here we demonstrate that lily *VERNALIZATION INSENSITIVE 3-LIKE 1* (*LoVIL1*) confers growth transition by mediating plasmodesmata opening via epigenetic repression of *CALLOSE SYNTHASE 3* (*LoCALS3*). Moreover, we found that a novel transcription factor, NUCLEAR FACTOR Y, SUBUNIT A7 (*LoNFYA7*), is capable of recruiting the LoVIL1–Polycomb Repressive Complex 2 (PRC2) and enhancing H3K27me3 at the *LoCALS3* locus by recognizing the CCAAT *cis*-element (Cce) of its promoter. The LoNFYA7–LoVIL1 module serves as a key player in orchestrating the phase transition from slow to fast growth in lily bulbs. These studies also indicate that *LoVIL1* is a suitable marker for the bud-growth-transition trait following dormancy release in lily cultivars.

Many plants in temperate climate zones have evolved to adapt to seasonal changes so that their buds/seeds sprout in spring, grow until autumn and undergo a period of rest, called dormancy, in winter¹. Dormancy, during which meristems in buds or embryos in seeds are mostly inactive, enables plants to withstand harsh environmental conditions, especially short days (SD) and low temperatures. Besides its ecological importance, dormancy is also an essential economic trait, as viviparous seeds (due to a lack of dormancy) or deeply dormant buds impair crop yields and are not acceptable to breeders.

Light and temperature are the key factors regulating plant dormancy^{1,2}. As a response to unfavourable external signals from the environment, plant internal signals, hormones and carbohydrates

are adjusted to maintain dormancy and prevent active growth¹. In poplar, SD negatively regulate the photoperiodic signalling proteins. First, SD suppress CONSTANS/FLOWERING LOCUST (CO/FT), leading to the suppression of *Like-AP1* (*LAPI*) and *AINTEGUMENTA-LIKE1* (*AIL1*) and resulting in growth cessation. Following this, abscisic acid (ABA) is upregulated and the gibberellic acid (GA) pathway is repressed, causing the induction of *CALLOSE SYNTHASE* (*CALS*) and dormancy^{3–5}.

Long-term cold treatment (LTCT) releases dormancy by decreasing ABA. This is accompanied by reduction of sugar conversion and activation of respiration^{6,7}. In poplar, LTCT promotes dormancy release by upregulating the expression of *EARLY BUD-BREAK1* (*EBB1*) and down-regulating *SHORT VEGETATIVE PHASE-Like* (*SVL*), which represses ABA

¹Beijing Key Laboratory of Development and Quality Control of Ornamental Crops, Department of Ornamental Horticulture, China Agricultural University, Beijing, China. ²Institute of Grassland, Flowers, and Ecology, Beijing Academy of Agriculture and Forestry Sciences, Beijing, China. ³Institute of Biotechnology, Fujian Academy of Agricultural Sciences, Fuzhou, China. ⁴Institute of Floriculture, Liaoning Academy of Agricultural Sciences, Shenyang, China. ⁵Department of Life Sciences, Ben-Gurion University of the Negev, Beer Sheva, Israel. ⁶Department of Biological Sciences, University of Toronto Scarborough, Toronto, Ontario, Canada. ⁷Department of Cell and Systems Biology, University of Toronto, Toronto, Ontario, Canada. ⁸These authors contributed equally: Wenqiang Pan, Jingru Li, Yunpeng Du. ✉e-mail: jianwu@cau.edu.cn

synthesis that in turn promotes cell division and communication^{4,8}. In addition, LTCT is involved in histone modifications during dormancy release in some species⁹. *DORMANCY-ASSOCIATED MADS-box (DAM)* genes are master regulators of dormancy in Rosaceae such as peach, cherry and apple trees. In peach, downregulation of *DAM6* overlaps with downregulation of trimethylation of histone H3 at Lys4 (H3K4me3) and upregulation of trimethylation of histone H3 at Lys27 (H3K27me3) at its locus during dormancy release under LTCT⁹. However, the mechanism is far from understood.

In recent years, it was demonstrated that restoring intercellular communication in shoot apical meristems (SAMs) by opening plasmodesmata (PD) accelerates bud dormancy release and growth in poplar, while blocking PD results in bud dormancy¹⁰. In potatoes, callose is deposited around the PD, blocking the tuber-inducing activity in aerial nodes and maintaining axillary bud dormancy by reduced tuberigen proteins and sucrose¹¹. Callose is a β-1,3 glucan polymer derived from uracil-diphosphate glucose and plays a critical role in plant development and stress response. The dynamic transformation of callose, regulated by β-1,3 glucan synthase and β-1,3 glucanases, is the key to controlling intercellular PD¹². In poplar and birch buds, callose blocks PD trafficking during dormancy when ABA is induced, but LTCT induces the recovery of cytoplasmic transport by increasing β-1,3-glucanase levels, which promotes callose degradation¹². Moreover, PD reset contributes to vascular bundle opening, leads to the import of *FLOWERING LOCUS T (FT)* and *CENTRORADIALIS-LIKE 1 (CENL1)* to the SAM and further promotes bud development, such as elongation and morphogenesis. Clearly, intercellular communication is essential for plant dormancy release and bud development. But there is still much to learn about LTCT-induced PD trafficking, specifically in regard to epigenetic modifications.

LTCT is involved not only in bud dormancy but also in vernalization, a process in which flowering is hastened following extended cold exposure. Given the downregulation of floral repressors or upregulation of *FT* by LTCT, there are shared features between dormancy release and vernalization in some woody plant taxa including *Populus* and Rosaceae¹². VERNALIZATION INSENSITIVE 3 (VIN3) is a component of the Polycomb Repressive Complex 2 (PRC2) and increases H3K27me3 levels on floral repressor loci under LTCT^{13,14}. Recent studies have shown that two clock proteins CIRCADIAN CLOCK ASSOCIATED 1 (CCA1) and LATE ELONGATED HYPOCOTYL (LHY), as well as NTM1-LIKE 8 (NTL8) protein, are involved in plant perception of LTCT-activated VIN3 in *Arabidopsis*^{15,16}. Upon removal of vernalization treatments, *VIN3* is silenced by the PRC2 complex and by PRC1, from which the H3K9me2 and H3K27me3 are enhanced on *VIN3* locus¹⁷. VERNALIZATION INSENSITIVE LIKE1 (VIL1) is a homologue of VIN3 and is involved in ABA response, stress tolerance (heat and low oxygen), floral transition and cell differentiation^{18–21}. In *Arabidopsis*, VIL1 is also involved in vernalization-induced flowering via epigenetic regulation of *FLOWERING LOCUS C (FLC)* and *FLOWERING LOCUS M (FLM)*²². *Arabidopsis vil1* mutants exhibit hypersensitivity to ABA and delay seed germination due to increased ABA INSENSITIVE 3 (ABI3)¹⁹. VIL1 is capable of fine-tuning the timely repression of *ABI3* in seeds by PRC2-mediated H3K27me3 (ref. 19). In addition, VIL1 is involved in chromatin remodelling by forming a chromatin loop at the growth-promoting gene locus, interacting with the active form of phytochrome B and recruiting PRC2 (ref. 23). Given that PRC2 has no inherent DNA binding specificity, there must be transcription factors (TFs) that bind to *cis*-regulatory regions and recruit PRC2. Recent studies have identified several TFs that recruit PRC2 complexes, including C2H2 zinc-finger (ZnF) family, APETALA2-like (AP2) family, BASIC PENTACysteINE (BPC) family and telomere-repeat-binding factors (TRB) factors^{24,25}.

Lily (*Lilium* spp.) is a perennial bulb plant with both ornamental and edible values. In lilies, bud-growth transition following bulb dormancy is an important physiological trait that directly affects multiple developmental processes, including shoot meristem activity, flower

transition, inflorescence elongation and cut-flower quality. Although several transcriptomic and metabolic studies have been conducted on growth transition in lilies, the genetic evidence and molecular mechanisms are still missing^{26,27}. In this study, we identified a novel TF, LoNFYA7 (*Lilium* oriental NUCLEAR FACTOR Y, SUBUNIT A7), which recruits PRC2 by interacting with LoVIL1 in the lily cultivar Siberia. LoNFYA7 directly targeted *LoCALS3* locus and repressed its expression by recruiting LoVIL1-PRC2 during the growth transition from slow to fast growth following dormancy release, which promoted opening of PD, activated intercellular communication in the SAM and accelerated the growth transition. Notably, overexpression of *LoVIL1* generated an evergrowing lily, which does not undergo dormancy, suggesting that vernalization genes are involved in regulating growth transition.

Results

Bud development in lily bulbs during postharvest storage

For the lily cultivar Siberia, freezing (-1.5°C) and cold (4°C) temperatures are widely used in long-distance shipping and on-spot postharvest storage, respectively. Under LTCT, central buds in the bulbs grew at a very slow speed and grew even slower at -1.5°C than at 4°C (Extended Data Fig. 1a). Given that cold exposure period is correlated with plant growth after dormancy release, we investigated bud growth in plants developing from bulbs exposed to different lengths of storage at 4°C . Freshly harvested bulbs with less than 2 weeks of cold storage did not sprout for over 100 d (Extended Data Fig. 1b,c). In contrast, bulbs stored for over 8 weeks could totally sprout; the central bud elongated up to approximately two-thirds of the height of the entire bulb and sprouting occurred about 3 weeks after planting, without effects on plant height (Fig. 1a,b and Extended Data Fig. 1b,c). When placed at 12°C for 2 weeks after 8 weeks of cold storage, the shoot meristem started the transition into flower meristem (Extended Data Fig. 1d). These results confirm that cold exposure induces sprouting, bud development following bulb dormancy release and floral transition (vernalization) in the cultivar Siberia.

To better understand the growth transition following bulb dormancy release in the lily Siberia, we performed transcriptome sequencing in the SAM of central buds at 0 and 8 weeks of LTCT (Fig. 1a). We found a total of 24,672 differentially expressed genes (DEGs), of which 12,045 were upregulated and 12,627 were downregulated (Fig. 1c). Gene set enrichment analysis (GSEA) showed that DEGs related to histone lysine methylation and glucan metabolic pathways were enriched (Fig. 1d). Callosic plugs called dormancy sphincters control PD closure and are associated with dormancy induction⁴. Moreover, the myosin inhibitor, 2,3-butanedione-monoxime (BDM), as well as the callose biosynthesis inhibitor deoxy-D-glucose (DDG), promote intercellular transport through PD in *Tradescantia*, while the myosin ATPase-blockers, *N*-ethylmaleimide (NEM), has the opposite effect²⁸. As intercellular communication is required for sugar transport and messenger (m)RNA trafficking²⁹, we first treated dormant bulblets with the abovementioned PD-associated chemical reagents and observed their effects on growth transition. As we expected, both 1 mM DDG and 1 mM BDM dramatically accelerated bud growth in lily bulblets, whereas 1 mM NEM inhibited growth (Fig. 1e,f).

Next, we tracked the intercellular/symplastic transport of sugars in SAMs by using carboxyfluorescein diacetate (CFDA). Both BDM and DDG promoted symplastic transport in SAMs, while NEM had a negative effect (Extended Data Fig. 2). These results show that intercellular communication is associated with growth transition in lily.

Last, we inspected the PD state and the cell-cell communication in the SAM of dormant buds (DBs, with 0 weeks of LTCT) and growth-phase-transited bulblets (GTBs, with 8 weeks of LTCT). By using transmission electron microscopy (TEM), we found that the PD were closed in DBs but open in GTBs (Fig. 1g). We further analysed callose deposition in SAM cells with aniline blue staining. The fluorescence intensity in the SAMs of DBs was significantly higher than in those of GTBs (Fig. 1h).

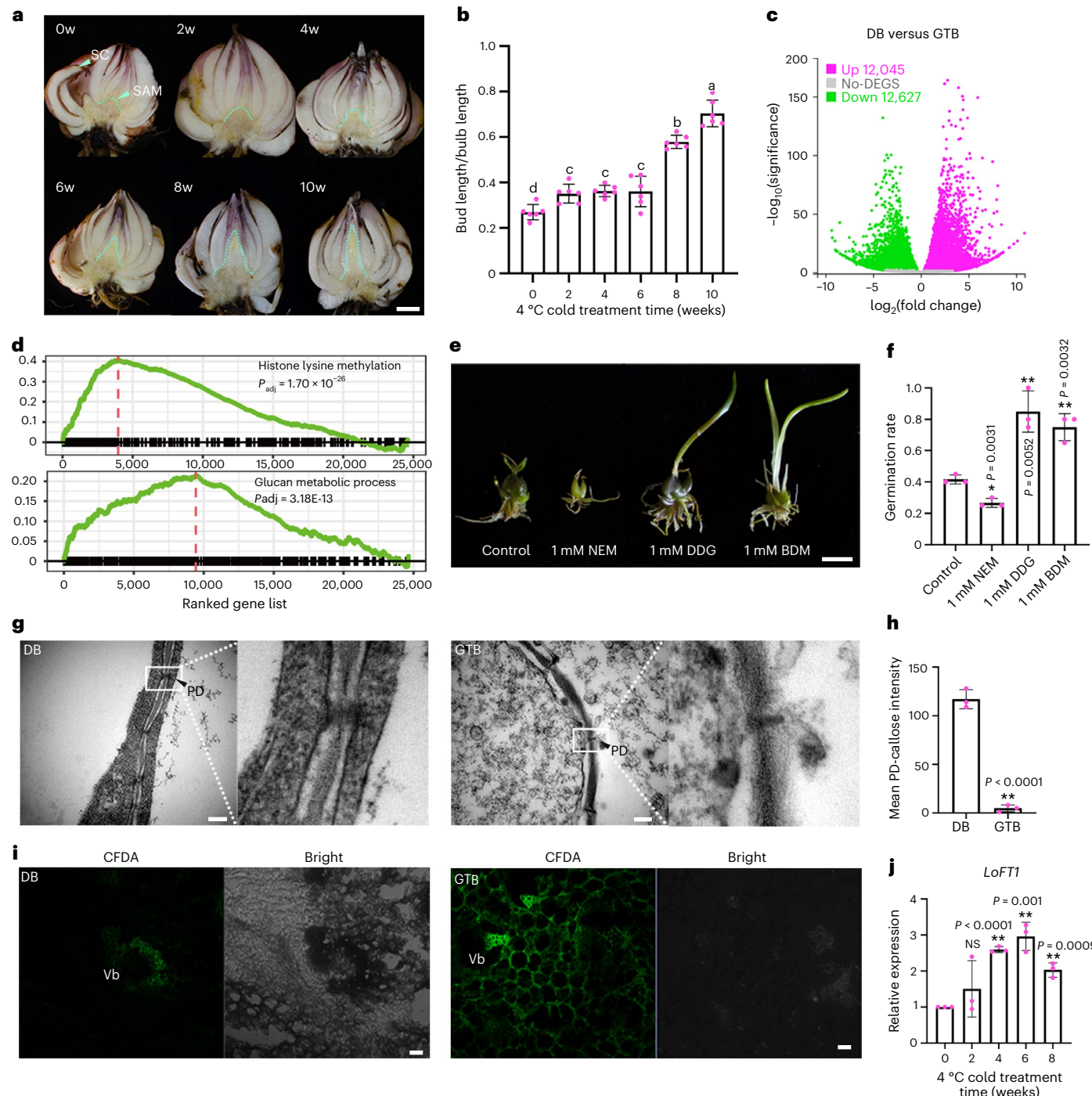


Fig. 1 | The crucial role of intercellular communication during bud-growth transition in lily bulbs. **a**, Morphological characterization of central bud outgrowth in lily cv. Siberia over 0–10 weeks (w) under 4 °C. Scale bar, 1 cm. **b**, Central bud/bulb length ratio. Data are presented as mean ± s.d. of 6 biological replicates ($n = 5$ bulbs per sample). Different letters above bars indicate significant differences ($P = 0.0001$) determined using ANOVA with Turkey's HSD tests for pairwise comparisons. **c**, Volcano plot comparing DB and GTB differential expression. Significant DEGs (two-sided Student's t -test, Benjamini–Hochberg false discovery rate adjusted $P < 0.05$, |fold change| > 2.0) are marked in magenta (upregulated) and green (downregulated). Three biological replicates per stage. **d**, Enriched pathways in central buds during growth transition were identified using GSEA. Significance was adjusted using Benjamini–Hochberg false discovery rate. **e,f**, Germination of deep dormant bulbs (e) grown on MS medium (control) or treated with NEM, BDM or DDG. Evaluation of germination rate (f) was done after 4 weeks based on leaf development. Data are presented as mean ± s.d. of 3 replicates ($n = 20$ bulbs per sample). A two-sided Student's t -test was used. Scale bar, 1 cm. **g**, TEM micrographs of central bud SAMs in DB and GTB. DB shows electron-dense dormancy sphincters associated with PD, whereas GTB lacks these structures. Scale bars, 0.2 μ m. **h**, Callose levels in PD decreased in central bud SAMs during growth transition. Aniline blue staining and ImageJ software were used for quantification. Data are presented as mean ± s.d. of 3 biological replicates ($n = 7$ SAMs per stage; two-sided Student's t -test).

i, Sugar symplastic transport visualized using CFDA in central buds of DB and GTB. CFDA fluorescence was confined to vascular bundles (Vb) in DB, but extended to parenchyma cells in GTB. Consistent results were obtained in at least 3 independent bulbs at the same stage. Scale bars, 20 μ m. **j**, *LoFT1* expression in SAMs was assessed by RT-qPCR during cold storage at 4 °C from 0 to 8 weeks. Data are presented as mean ± s.d. of 3 biological replicates ($n = 3$ SAMs per stage; two-sided Student's t -test; NS, not significant). SC, scales.

and Supplementary Fig. 1), showing more callose deposition in DBs compared with GTBs. Given that lily SAMs consist of parenchyma cells, symplastic transport is essential for SAM development. Therefore, we mimicked the symplastic transport of sugars by using CFDA during the growth transition. CFDA fluorescent signals in the SAM of DBs were much lower than those in GTBs (Fig. 1*j*). Since *FT* mRNA is involved in plant growth and vernalization in perennials and is also delivered to SAM via symplastic transport³⁰, we assessed *LoFT1* expression in the lily SAM by quantitative reverse transcription PCR (RT-qPCR). *LoFT1* expression continually accumulated along with LTCT (Fig. 1*j*), supporting to a certain extent previous findings that intercellular communication via PD is gradually recovered by LTCT and that floral transition occurs in parallel with the accumulation of *LoFT1* mRNA.

***LoVIL1* positively regulates growth transition**

To address whether vernalization-related histone modification is involved in the growth transition, we selected *LoVIL1*, which was induced by LTCT, as a candidate from the transcriptome database (Supplementary Fig. 2). We first detected *LoVIL1* expression in SAM by *in situ* hybridization. *LoVIL1* was barely expressed in the SAM of DBs before LTCT, but its expression increased in both the SAM and the leaf-scale primordia in GTBs after LTCT (Fig. 2*a*). Similarly, *LoVIL1* expression increased in SAMs along with LTCT (Fig. 2*b*). Moreover, *LoVIL1* was not expressed in roots, stamens, inner petals or filaments but is abundant in pistils, scales, leaves, ovaries and buds (Supplementary Fig. 3).

Next, we investigated the role of *LoVIL1* in the growth transition in lilies using virus-induced gene silencing (VIGS). We agroinfiltrated dormant bulbs and stored them at 4 °C for 8 weeks and detected virus-infected and *LoVIL1*-silenced bulbs with *COAT PROTEIN* and *VIL1* primers, respectively (Extended Data Fig. 3). Compared with the TRV2 control, silencing *LoVIL1* resulted in delayed central bud growth and shorter buds (Fig. 2*c,d*), increased callose deposited on PD, a large number of closed PD in the SAM (Fig. 2*e,f* and Supplementary Fig. 4) and decreased symplastic transport of sugars as well as a decreased *LoFT1* mRNA level in the SAMs (Fig. 2*l,m*). Silencing *LoVIL1* further caused delayed sprouting and flowering time (Extended Data Fig. 3). Notably, we found shorter inflorescences and fewer flower numbers in TRV2-*LoVIL1* lines, but leaf number was not affected (Extended Data Fig. 3*f–i*). These results showed that *LoVIL1* plays a positive role in the bud-growth transition in lily by decreasing callose deposition on PD and promoting cell-cell communication in the SAMs. Furthermore, *LoVIL1* increases *LoFT1* mRNA level and promotes flower transition, possibly through the import of *LoFT1* mRNA to the apical meristem region.

Next, we further characterized the *LoVIL1* function by generating transgenic lily plants overexpressing *LoVIL1* (OE-*LoVIL1*; Extended Data Fig. 4). Wild-type (WT) lily went into dormancy after 8 months of growth in jars and displayed leaf senescence on inner scales, no generation of young leaves from the central scales and blocked PD in SAMs (Fig. 2*g–i* and Supplementary Fig. 5). However, OE-*LoVIL1* lines

skipped the dormant phase and showed evergrowing phenotypes in jars, as they kept generating new leaves from central scales (Fig. 2*g* and Extended Data Fig. 4). This phenotype was accompanied by decreased closure of the PD in the OE-*LoVIL1* lines compared with the WT (Fig. 2*h,i*). Enforcing blocking of PD by NEM restored the bulb dormancy trait in OE-*LoVIL1* lines (Fig. 2*j,k*). In addition, several other phenotypes were also observed in the OE-*LoVIL1* lines, including purple and curly leaves, early senescent leaves on outer scales and faster growth with increased scale production (Fig. 2*g* and Extended Data Fig. 4).

In summary, *LoVIL1* expression is stimulated in the SAMs of lily bulbs by cold storage, which accelerates the growth transition by promoting cell-cell communication through PD and increasing *LoFT1* mRNA accumulation.

***LoVIL1* downregulates *LoCALS3* for cell-cell communication**

To further study the relationship between *LoVIL1* and callose deposition in PD, we first investigated callose biosynthesis genes in the transcriptome database. We identified five DEGs of the *CALS* family: *LoCALS3*, *LoCALS5*, *LoCALS7*, *LoCALS10* and *LoCALS12* (Fig. 3*b* and Supplementary Fig. 6). Verified by RT-qPCR, *LoCALS3* was the only DEG whose expression decreased in the SAM during LTCT (Fig. 3*b* and Supplementary Fig. 6). We also detected the expression pattern in organs of the central buds at DB and GTB stages by *in situ* hybridization. *LoCALS3* was expressed at high levels in the arrested SAM region and leaf-scale primordia at the dormant stage (Fig. 3*a*). When the growth phase was transitioned in bulbs (GTBs), *LoCALS3* expression decreased in the active SAM region and leaf-scale primordia (Fig. 3*a,b*). The expression pattern of *LoCALS3* was opposite to that of *LoVIL1* (Figs. 2*b* and 3*b*), so we hypothesize that *LoVIL1* negatively regulates *LoCALS3* expression. To test this hypothesis, we examined *LoCALS3* expression in *LoVIL1*-overexpressed lily plants and calluses (Fig. 3*c* and Supplementary Fig. 7). The decrease in *LoCALS3* expression in tissues of plants overexpressing *LoVIL1* is in agreement with the assumption that *LoVIL1* represses *LoCALS3* expression. Moreover, we found that silencing of *LoVIL1* upregulated *LoCALS3* expression (Fig. 3*d*). These results imply that *LoCALS3* may be critical for callose synthesis and may be involved in the growth transition mediated by *LoVIL1* in lily bulbs. To examine the role of *LoCALS3* in the growth transition in lily bulbs, we conducted a VIGS assay using dormant bulbs. Compared with the TRV2 control, silenced *LoCALS3* dramatically promoted central bud elongation after 6 weeks of cold storage, with central buds reaching two-thirds of the bulb length, indicating a faster growth transition (Fig. 3*e,f* and Supplementary Fig. 8). In addition, silencing of *LoCALS3* caused a 50% decrease of callose in PD and faster symplastic transport of sugars in SAMs (Fig. 3*g–i* and Supplementary Fig. 9). These features were accompanied by an increase in *LoFT1* accumulation (Fig. 3*j*). This indicates that *LoCALS3* negatively regulates growth transition in lily bulbs by increasing callose deposition in the PD and further blocking cell-cell communication. All these results show that *LoVIL1* promotes intercellular communication by

Fig. 2 | *LoVIL1* accelerates growth transition and promotes intercellular communication in lily. **a**, mRNA *in situ* hybridization of *LoVIL1* in SAMs of DB and GTB. Scale bars, 1 mm. **b**, *LoVIL1* expression patterns in SAMs during cold storage, as measured by RT-qPCR. Mean ± s.d. of 3 independent replicates ($n = 3$ SAMs per stage). Different letters above bars indicate significant differences ($P = 0.0001$) determined using ANOVA with Turkey's HSD tests for pairwise comparisons. **c,d**, Silencing of *LoVIL1* in dormant bulbs delays growth transition. Images were taken 8 weeks after infiltration (**c**). Scale bar, 2 cm. Representative images of 3 independent experiments are shown. Central buds of TRV2-*LoVIL1* bulbs grew slower than controls (**d**). Mean ± s.d. of 6 independent plants (two-sided Student's *t*-test). **e**, TEM microscopy of SAMs in TRV2- and TRV2-*LoVIL1* bulbs. More PD with electron-dense dormancy sphincters were found in TRV2-*LoVIL1* compared with TRV2 8 weeks after LTCT. Scale bars, 0.2 μ m. **f**, Abundant callose at PD in SAMs of TRV2-*LoVIL1* compared with TRV2 ($n = 6$ SAMs per replicate). **g**, Continuous development of leaves on the tip of the

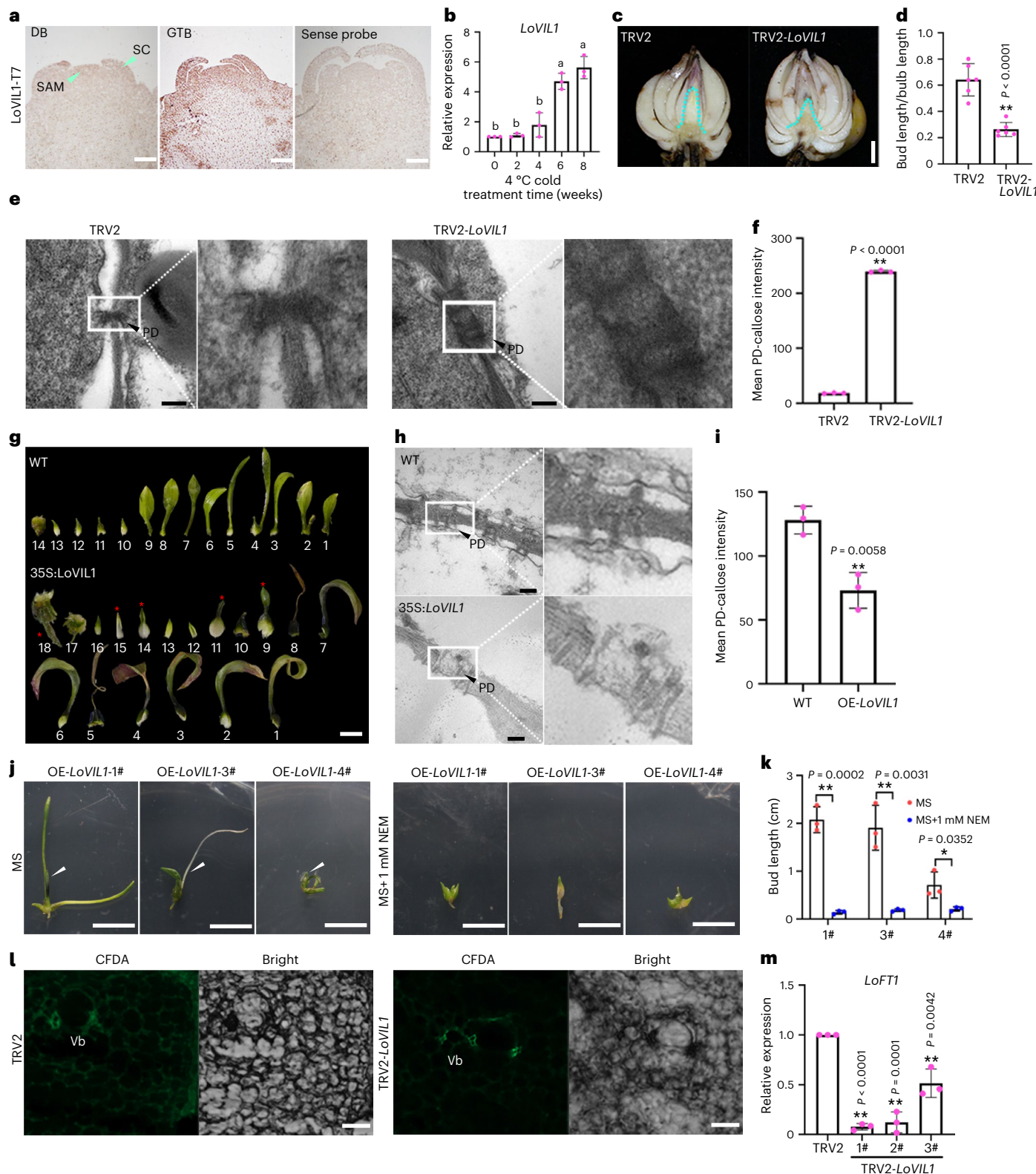
central scale in OE-*LoVIL1* lines, showing evergreen phenotypes and more scales. Scales peeled off from outer to inner parts, listed from right to left. Red asterisks indicate newly developed leaves. Scale bars, 1 cm. **h**, TEM micrographs of SAMs in WT and OE-*LoVIL1* bulbs. Scale bars, 0.2 μ m. **i**, Repression of callose in PD by *LoVIL1*. Mean ± s.d. of 3 different lines ($n = 11$ section slides per sample). **j**, NEM represses growth transition in OE-*LoVIL1* plants. Bulbs of OE-*LoVIL1* lines were grown on MS or MS containing NEM for 4 weeks. Scale bars, 1 cm. **k**, Bud length of OE-*LoVIL1* lines grown on MS media with or without NEM ($n = 3$ plants per line). **l**, Visualization of sugar symplastic transport using CFDA in central buds of TRV2 and TRV2-*LoVIL1*. CFDA was less expanded to the surrounding parenchyma cells in TRV2-*LoVIL1* compared with TRV2. Consistent results in at least 3 independent bulbs. Scale bars, 20 μ m. **m**, Reduced *LoFT1* mRNA levels in SAMs of TRV2-*LoVIL1*. Three independent SAMs were used for RT-qPCR. Data in **f**, **i**, **k** and **m** represent mean ± s.d. of 3 biological replicates (two-sided Student's *t*-test).

repressing *LoCAL3* expression in SAMs during the growth transition following dormancy release in lily bulbs.

LoNFYA7 inhibits cell–cell communication with LoVIL1

In angiosperms, VIL1 is a component of the PRC2 complex¹⁹. To validate its conserved function in lily, we performed yeast two-hybrid (Y2H) and split-luciferase assays, showing that LoVIL1 interacts with LoMSI1 in yeast and in planta (Extended Data Fig. 5a,b). Moreover, we

also confirmed that LoVIL1 is localized in the nucleus and is involved in the upregulation of H3K27me3 by transiently overexpressing *LoVIL1* in *Nicotiana benthamiana* leaves (Extended Data Fig. 6). This established that LoVIL1 is a subunit of PRC2. Since the LoVIL1–PRC2 complex does not directly bind DNA, we conducted Y2H screening with the lily complementary (c)DNA library made from dormant bulbs to find TFs capable of recruiting the complex. To this end, we used the full length of LoVIL1 as the prey for Y2H screening and found 10



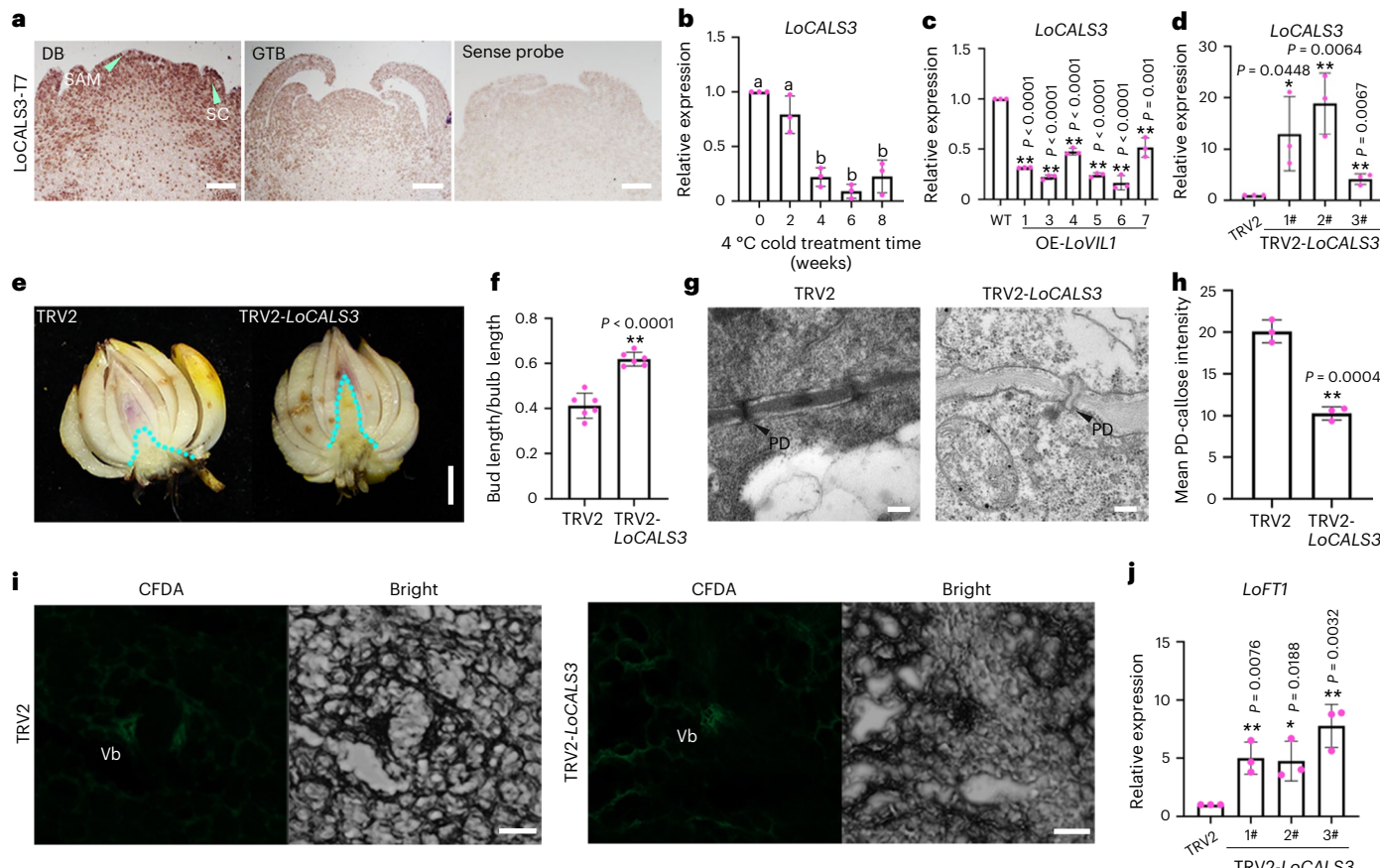


Fig. 3 | LoCALS3 delays growth transition by blocking intercellular communication in lily. **a**, mRNA in situ hybridization of *LoCALS3* in SAMs of DB and GTB. Scale bars, 1 mm. **b**, Expression patterns of *LoCALS3* in SAMs during cold storage (0–8 weeks of LTCT) as measured by RT-qPCR. Data are presented as mean ± s.d. of 3 independent replicates ($n = 3$ SAMs per sample). Different letters above bars indicate significant differences ($P = 0.0001$) determined by ANOVA with Turkey's HSD tests for pairwise comparisons. **c,d**, Comparison of *LoCALS3* expression levels in OE-*LoVIL1* plants (**c**) and in SAMs of TRV2-*LoCALS3* (**d**) by RT-qPCR. Data are presented as mean ± s.d. of 3 biological replicates (two-sided Student's *t*-test). **e,f**, Silencing of *LoCALS3* in dormant bulbs accelerates growth transition. Images were taken 6 weeks after infiltration (**e**). Scale bar, 2 cm. The blue-green dotted line outlines the central bud. Representative images of 3 independent experiments are shown. Central buds of TRV2-*LoCALS3* bulbs exhibited significantly faster growth than TRV2 (**f**). Data are presented

as mean ± s.d. of 6 independent plants (two-sided Student's *t*-test). **g**, TEM microscopy of SAMs in central buds of TRV2- and TRV2-*LoCALS3* bulbs. A few PD with electron-dense dormancy sphincters were still observed in TRV2, while they were absent in TRV2-*LoCALS3* after 8 weeks of LTCT. Scale bars, 0.2 μ m. **h**, Callose deposition in PD was significantly reduced in SAMs of TRV2-*LoCALS3* bulbs compared with TRV2. Data are presented as mean ± s.d. of 3 biological replicates ($n = 6$ SAMs per replicate; two-sided Student's *t*-test). **i**, Simulation of symplastic transport using CFDA in central buds of TRV2 and TRV2-*LoCALS3* bulbs. CFDA fluorescence was less expanded to the surrounding parenchyma cells in TRV2 compared with the TRV2-*LoCALS3*. Consistent results were obtained in at least 3 independent bulbs. Scale bars, 20 μ m. **j**, Abundant *LoFT1* mRNA levels were observed in SAMs of TRV2-*LoCALS3* bulbs compared with TRV2. Three different lines were used for RT-qPCR. Data are presented as mean ± s.d. of 3 biological replicates (two-sided Student's *t*-test).

potentially interacting proteins, among which a member of the Nuclear Factor Y (NF-Y) family was identified and named *LoNFYA7* (Fig. 4a and Supplementary Figs. 10 and 11). Of notice, members of ZnF, AP2, BPC and TRB are known to recruit PRC2, but whether NF-YA members are involved in recruiting PRC2 is still unknown. Here we found that *LoNFYA7* can interact with *LoVIL1* and its PHD domain in yeast (Fig. 4b), and the interaction between these two proteins was further confirmed in planta using the split-luciferase assay and bimolecular fluorescence complementation (BiFC) assay (Fig. 4c,d). In addition, we performed fluorescence resonance energy transfer (FRET) assay and confirmed the interaction in vitro (Fig. 4e). These results indicate that *LoNFYA7* is able to recruit the PRC2 complex by physically interacting with *LoVIL1*.

To further characterize the role of *LoNFYA7* during the growth transition, we detected its expression by in situ hybridization and RT-qPCR. Similar to *LoCALS3*, *LoNFYA7* was expressed at high levels in dormant central buds, especially in the SAM region and leaf primordia, and its expression decreased in GTBs (Fig. 4f,g). Next, we investigated the effect of *LoNFYA7* on growth transition using the VIGS assay in

dormant lily bulbs. Silencing of *LoNFYA7* caused faster central bud growth after 6 weeks and 10 weeks of cold storage (Fig. 4j,k and Supplementary Fig. 12). Interestingly, the effect of silencing *LoNFYA7* on bud growth appears to be milder than that of silencing *LoCALS3* or *LoVIL1* (Figs. 2c,d, 3e,f and 4j,k). Silencing of *LoNFYA7* caused a decrease of about one-third in the callose in PD, an increase of the *LoFT1* mRNA levels and active symplastic transport of sugars in SAM (Fig. 4l-o and Supplementary Fig. 13), indicating that *LoNFYA7* negatively regulates growth transition in lily bulbs by increasing callose deposition on PD and further obstructing intercellular communication.

LoNFYA7 directly regulates *LoCALS3* expression with *LoVIL1*

To study whether *LoNFYA7* regulates *LoCALS3* expression, we first detected *LoCALS3* expression in *LoNFYA7*-overexpressing calluses and SAMs of TRV2-*LoNFYA7* lines. Overexpressing *LoNFYA7* led to increased *LoCALS3* mRNA levels, but silencing *LoNFYA7* reduced *LoCALS3* expression (Fig. 4h,i and Supplementary Fig. 14), suggesting that *LoNFYA7* itself can positively regulate *LoCALS3* expression.

Given that the NF-Y TFs directly bind CCAAT *cis*-elements (*Cces*), we speculated that LoNFYA7 directly binds the *LoCALS3* promoter after finding five *Cces* within the 2 Kb upstream genomic sequence from the transcription start site (Fig. 6a). We used the 3 tandem repeats of the promoter sequence (-249 bp to -239 bp; referred to as transcription start site) as the bait, fused with Aureobasidin A resistant (AbA^r) reporter and tested the interaction between the promoter and LoNFYA7 protein in yeast. LoNFYA7 could directly bind the promoter and activate the AbA^r reporter that allowed yeast cells to grow on AbA^r-selected media (Fig. 5a).

To validate the specific binding on the *Cce* of the *LoCALS3* promoter, we employed the electrophoretic mobility shift assay (EMSA). The result indicated that LoNFYA7 binds the *Cce* in the *LoCALS3* promoter and tetranucleotide mutations of the *cis*-element abolished the binding ability of LoNFYA7 (Fig. 5b).

To further determine the effect of LoNFYA7 and LoVIL1 on the *LoCALS3* promoter, we performed a dual-luciferase assay by transient expression in calluses. Transient overexpression of LoNFYA7 alone activated the *LoCALS3* promoter (Fig. 5c–e). Moreover, we also found that LoNFYA7 could bind the region containing the *Cces* on the *LoCALS3* promoter in vivo by using chromatin immunoprecipitation quantitative real-time PCR (ChIP-qPCR) (Fig. 5h). Together with previous results (Figs. 4h,i and 5a,b), these data indicate that LoNFYA7 binds the *LoCALS3* promoter and upregulates *LoCALS3* expression. Notably, when both LoNFYA and LoVIL1 were present, *LoCALS3* promoter activity was dramatically inhibited (Fig. 5d,e); silencing of LoNFYA7 relieves the inhibition of LoVIL1 on *LoCALS3* promoter activity and *LoCALS3* expression (Fig. 5f,g). These results suggest that LoNFYA7 binds the *LoCALS3* promoter and recruits LoVIL1-PRC2 to further downregulate *LoCALS3* expression.

LoNFYA7 recruits LoVIL1 to repress *LoCALS3* via H3K27me3

The results shown so far suggest that the interaction between LoVIL1 and LoNFYA7 may participate in the epigenetic repression of *LoCALS3* during the growth transition following dormancy release in lily bulbs. To explore the relationship between H3K27me3 and *LoCALS3*, we compared the H3K27me3 levels on *LoCALS3* locus during the growth transition by using ChIP-qPCR with anti-H3K27me3. H3K27me3 levels increased dramatically on P1 and P2 regions with NFYA binding sites (CCAAT), while no changes occurred at P3 region without NFYA binding site (Fig. 6a,b), suggesting that H3K27me3 is involved in regulating *LoCALS3* expression during the growth transition. To support our hypothesis that LoVIL1-PRC2 contributes to H3K27me3 on *LoCALS3* locus, we detected H3K27me3 levels in *LoVIL1*-overexpressed transgenic lily and transiently overexpressed SAMs and obtained the same results: LoVIL1 promoted H3K27me3 on *LoCALS3* P1 and P2 regions with NFYA binding sites (Fig. 6c,d). The results are in accordance with the previous data showing that overexpression of *LoVIL1* repressed *LoCALS3*

expression (Fig. 3c and Supplementary Fig. 7b), implying that *LoNFYA7* mediates H3K27me3 modification on *LoCALS3* locus by recruiting LoVIL1-PRC2. To investigate whether LoNFYA7 is able to enhance the H3K27me3 levels on *LoCALS3* locus, we detected H3K27me3 levels in *LoNFYA7*-overexpressing SAMs of bulbs. H3K27me3 was enriched on both P1 and P2 regions in *LoNFYA7*-overexpressing SAMs but did not change in the P3 region (Fig. 6d), showing that *LoNFYA7* is able to promote H3K27me3. Moreover, co-overexpression of *LoNFYA7* and *LoVIL1* can sharply increase the H3K27me3 levels on these regions, compared with overexpression of the single genes (Fig. 6d). Silencing of *LoNFYA7* in *LoVIL1*-overexpressing SAMs significantly reduced H3K27me3 levels at P1 and P2 regions compared with those of overexpression of *LoVIL1* (Fig. 6e), showing the important role of LoNFYA7 in recruiting LoVIL1. The enhanced H3K27me3 on *LoCALS3* locus seems to conflict with increased *LoCALS3* in *LoNFYA7*-overexpressed calluses (Fig. 4h). Taking into account that NFYA TFs are involved in H3K9ac by competing with histone deacetylase GmHDA13 in *Glycine max*³¹, we examined the potential role of H3K9ac in the process of growth transition and in *LoNFYA7*-overexpressed SAMs. As expected, H3K9ac was dramatically decreased at P1 and P2 regions during the growth transition and in *LoNFYA7*-silenced SAMs (Fig. 6f,h) while being significantly increased in *LoNFYA7*-overexpressed SAMs (Fig. 6g); LoNFYA7 competed with LoHDA14 in lily, regulating *LoCALS3* expression and histone modifications (H3K27me3 and H3K9ac) (Extended Data Fig. 7). These results suggest that LoNFYA7 fine-tunes *LoCALS3* expression via crosstalk balancing between H3K9ac and H3K27me3. To sum up, during the growth transition following bulb dormancy release, LoNFYA7 participates in recruiting LoVIL1-PRC2 to repress *LoCALS3* expression by increasing H3K27me3 on LoNFYA7-binding locus.

LoVIL1 correlation with growth transition in lily cultivars

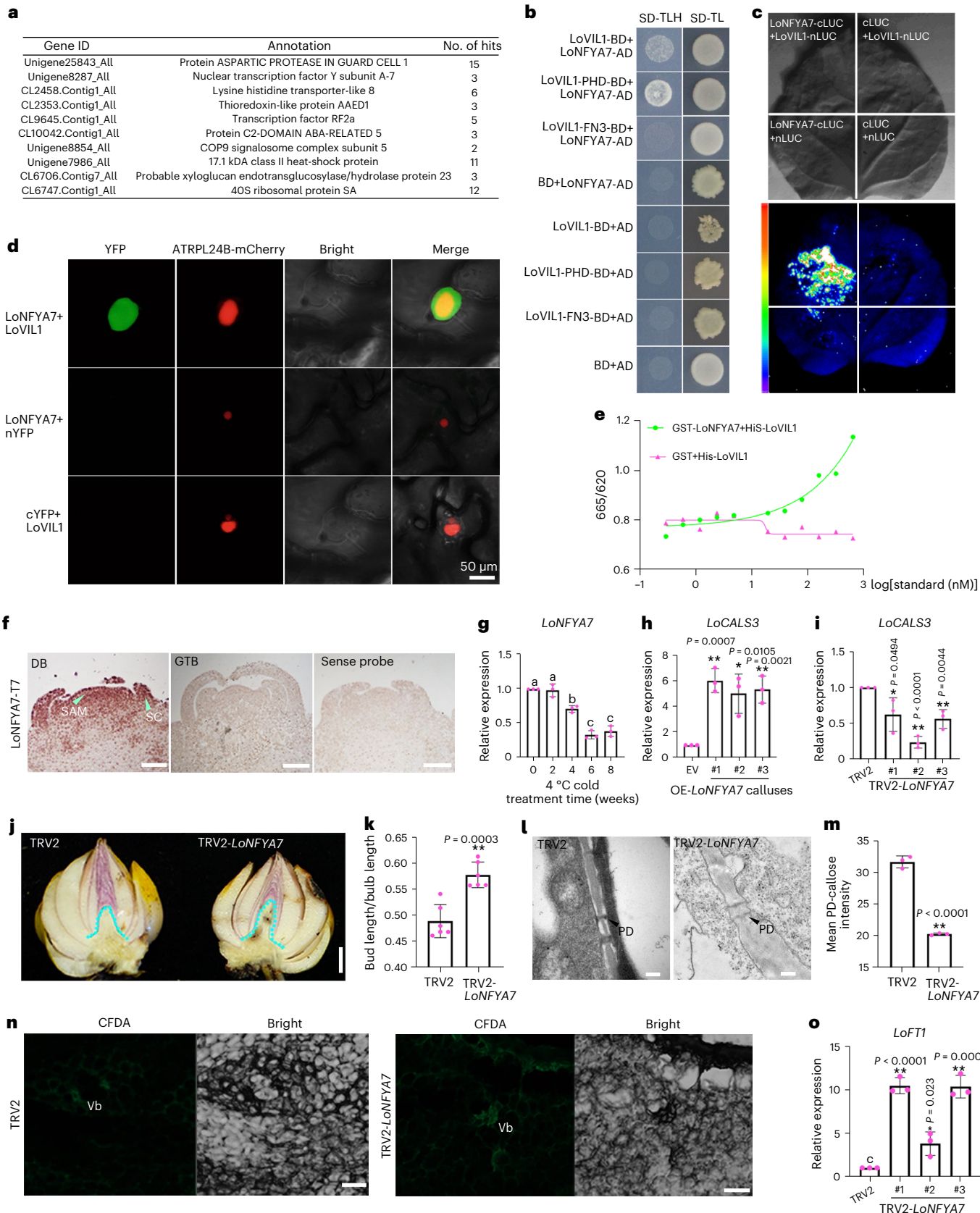
To investigate whether *LoVIL1*, *LoNFYA7* or *LoCALS3* can be potentially used for lily breeding, we first detected their expression in Asiatic lilies, that is, *L. lancifolium* characterized by a slow growth-transition trait and cultivar Must See with a faster growth-transition trait. When aboveground organs are withered, *L. lancifolium* bulbs enter into deep dormancy and the central bud remains near the basal plate. In contrast, the central bud of Must See is active and reaches two-thirds of bulb length (Fig. 7a). Moreover, bulbils in *L. lancifolium* keep dormant for about 3 months (Fig. 7b), but bulbils in Must See start to grow leaves and roots even when they are on the mother plants, showing a viviparous phenotype (Fig. 7c). We analysed the expression pattern of *LoVIL1*, *LoNFYA7* and *LoCALS3* in these two varieties at three time-points: the dormant stage when aboveground organs are withered, the growth-transited stage when bulbs are under 4 °C for 8 weeks and the sprouting stage when bulbs are under 12 °C for 2 weeks after being under 4 °C for 8 weeks. We found that (1) *LoVIL1* was consistently increased during the bud-growth transition in the two species.

Fig. 4 | LoVIL1 interactor, LoNFYA7, represses growth transition by blocking intercellular communication. **a**, Protein interactors of LoVIL1 identified through Y2H screening. Unigene8287-All is LoNFYA7 (Supplementary Fig. 11). **b**, Y2H validation of the interaction between LoVIL1 and LoNFYA7. Truncated forms of LoVIL1-PHD (1–224 amino acids) and LoVIL1-FN3 (189–623 amino acids) were used. **c,d**, *In planta* confirmation of the LoVIL1–LoNFYA7 interaction through split-luciferase assay (c) and BiFC (d) in *N. benthamiana* leaves. In c, bright fields (top) and dark fields (bottom) were shown, along with a color bar indicating luminescence intensity from weak (blue) to strong (red or white). Consistent results were confirmed in at least 3 independent experiments. Scale bar, 50 μm (d). **e**, *In vitro* confirmation of LoVIL1–LoNFYA7 interaction by FRET assay. Dots represent the means of 3 biological replicates ($n = 3$ samples per replicate). **f,g**, mRNA in situ hybridization of *LoNFYA7* in SAMs of DBs and GTBs. Scale bars, 1 mm. **g**, *LoNFYA7* expression in SAMs during cold storage. Mean ± s.d. of 3 biological replicates ($n = 3$ SAMs per sample). Different letters above bars indicate significant differences ($P = 0.0001$) determined using ANOVA with Turkey's HSD tests for pairwise comparisons. **h,i**, *LoCALS3* expression in transient

OE-*LoNFYA7* calluses (h) and in SAMs of TRV2-*LoNFYA7* bulbs (i). At least 3 different lines were used. Mean ± s.d. of 3 biological replicates (two-sided Student's *t*-test). EV, 3SS:GFP. **j,k**, Silencing of *LoNFYA7* in dormant bulbs accelerates growth transition. Images captured 6 weeks after infiltration (j). Scale bar, 2 cm. Representative images of 3 independent experiments are shown. Central buds of TRV2-*LoNFYA7* bulbs elongated earlier than those of TRV2 (k). Mean ± s.d. of 6 independent plants (two-sided Student's *t*-test). **l**, TEM microscopy of SAMs in central buds. A few PD with electron-dense dormancy sphincters were observed in TRV2, while they were absent in TRV2-*LoNFYA7* 8 weeks after LTCT. Scale bars, 0.2 μm. **m**, Callose deposition in PD was reduced in SAMs of TRV2-*LoNFYA7* bulbs compared with TRV2. Mean ± s.d. of 3 biological replicates ($n = 6$ SAMs per replicate; two-sided Student's *t*-test). **n**, Simulation of symplastic transport using CFDA in central buds of bulbs. CFDA was less expanded to the surrounding parenchyma cells in TRV2 compared with TRV2-*LoNFYA7*. Consistent results were obtained in at least 3 independent bulbs. Scale bars, 20 μm. **o**, Abundant *LoFTI* mRNA was observed in SAMs of TRV2-*LoNFYA7* tested by RT-qPCR. Mean ± s.d. of 3 biological replicates (two-sided Student's *t*-test).

In Must See, *LoVIL1* transcripts were always more abundant than in *L. lancifolium* and were maintained at high levels at the sprouting stage, whereas *LoVIL1* transcripts were reversely decreasing in *L. lancifolium* (Fig. 7d); (2) During the bud-growth transition and sprouting stages,

LoNFYA7 was gradually decreased in Must See while it did not change significantly in *L. lancifolium* (Fig. 7e); (3) *LoCALS3* maintained a low level of expression at all tested stages in Must See as opposed to high levels in *L. lancifolium* (Fig. 7f). Notably, we also observed earlier flower



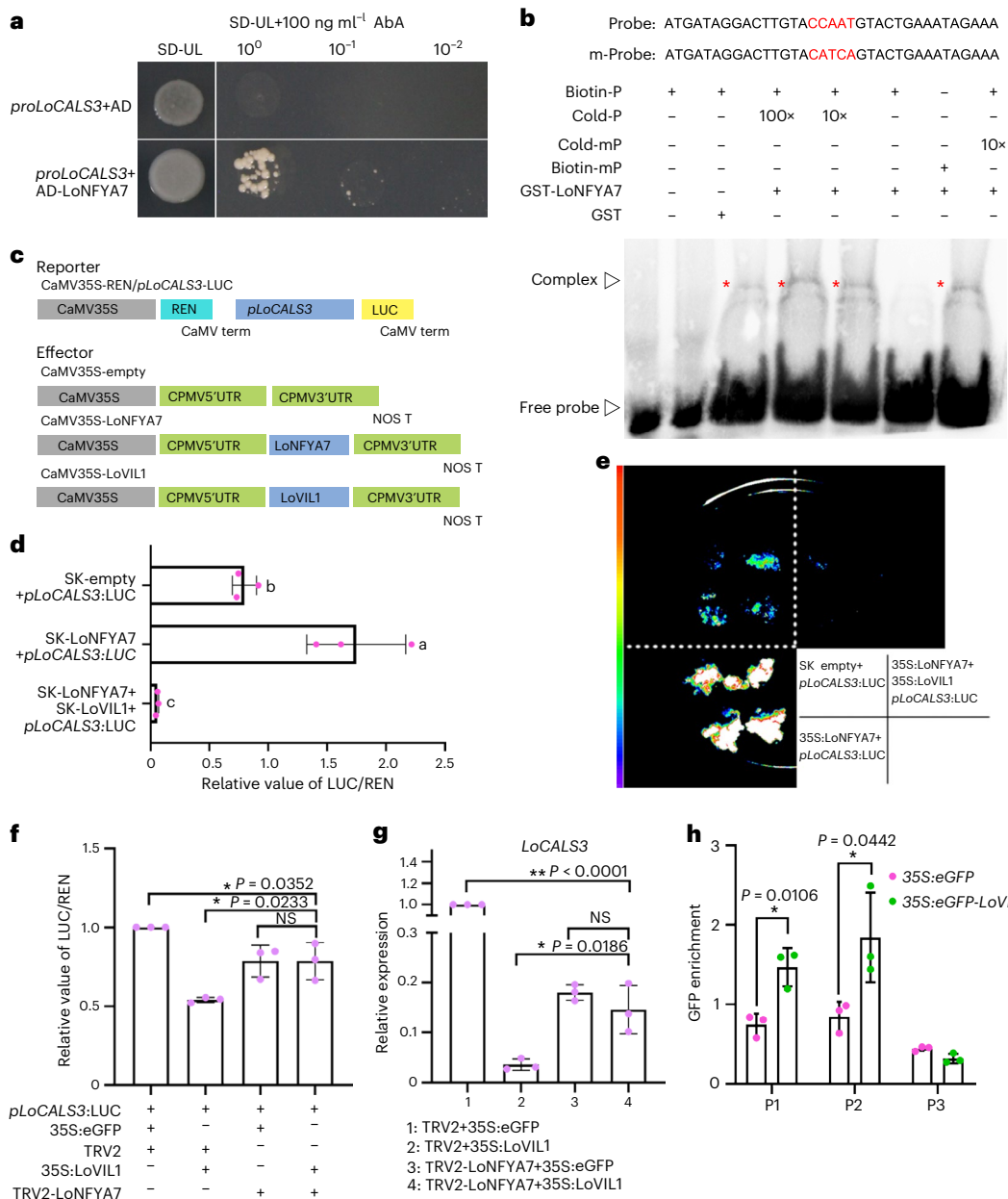


Fig. 5 | LoNFYA7 directly binds the LoCALS3 promoter and controls its expression. **a**, YIH validation of the interaction between LoNFYA7 and the LoCALS3 promoter. Empty pGADT7 served as the control (AD). AbA, Aureobasidin A. **b**, In vitro EMSA confirming direct binding of LoNFYA7 to the CCAAT motif (-261 bp to -227 bp) of the LoCALS3 promoter. The probe with a mutated CCAAT motif served as a control. Red letters in the probe indicate the CCAAT motif of the LoCALS3 promoter. Red asterisks indicate the binding complex. Consistent results were observed in 3 independent repeats. **c–e**, Validation of the LoNFYA7 interaction with the LoCALS3 promoter in lily calluses using the dual-luciferase assay. **c**, The LoCALS3 promoter (~1,301 bp to ~201 bp) was inserted into pGreenII 0800-LUC vector, with the empty pGreenII 62-SK vector as the control. **d**, The LUC/REN ratio of empty vector (SK) and LoCALS3 promoter combination was used for normalization (set to 1). Mean \pm s.d. of 3 biological replicates ($n = 6$ calluses/replicates). Different letters above bars indicate significant differences ($P = 0.0005$) determined using ANOVA with Turkey's HSD tests for

pairwise comparisons. **e**, Images taken on 3rd day after agroinfiltration using 4 independent calluses per sample. A color bar indicates luminescence intensity from weak (blue) to strong (red or white). **f**, Relief of LoCALS3 promoter activity inhibition upon silencing of LoNFYA7 in the LoVIL1-overexpressing SAMs. The LUC/REN ratio of the combination of 35S:eGFP/SK, TRV2 and pLoCALS3:LUC was used for normalization (set to 1). Mean \pm s.d. of 3 biological replicates ($n = 6$ SAMs per replicate; two-sided Student's *t*-test). **g**, Expression of LoCALS3 in lily SAMs. Mean \pm s.d. of 3 biological replicates (two-sided Student's *t*-test). **h**, RT-qPCR analysis of ChIP assay using chromatin extracted from transiently expressed 35S:eGFP-LoVIL1 and 35S:eGFP (negative control) calluses in lily. The LoCALS3 promoter regions P1, P2 and P3 (Fig. 6a) were tested. Antibodies against the GFP tag were used for IP. Enriched values were normalized to the level of input DNA and the relative fold enrichment over the empty vector is presented. Mean \pm s.d. of 3 biological replicates (two-sided Student's *t*-test).

bud development in Must See than in *L. lancifolium* (Extended Data Fig. 8a,b). Silencing of LoVIL1, LoNFYA7 or LoCAL3 in dormant bulbils of *L. lancifolium* showed phenotypes similar to those in Siberia (Extended Data Fig. 9). These results suggest that LoVIL1 is a good candidate for

an index of the growth transition following dormancy release and early flowering in lilies.

To further validate the potential usage of LoVIL1 in lilies, we tested its transcriptional levels in 7 different cultivars of Oriental lilies (Fig. 7g).

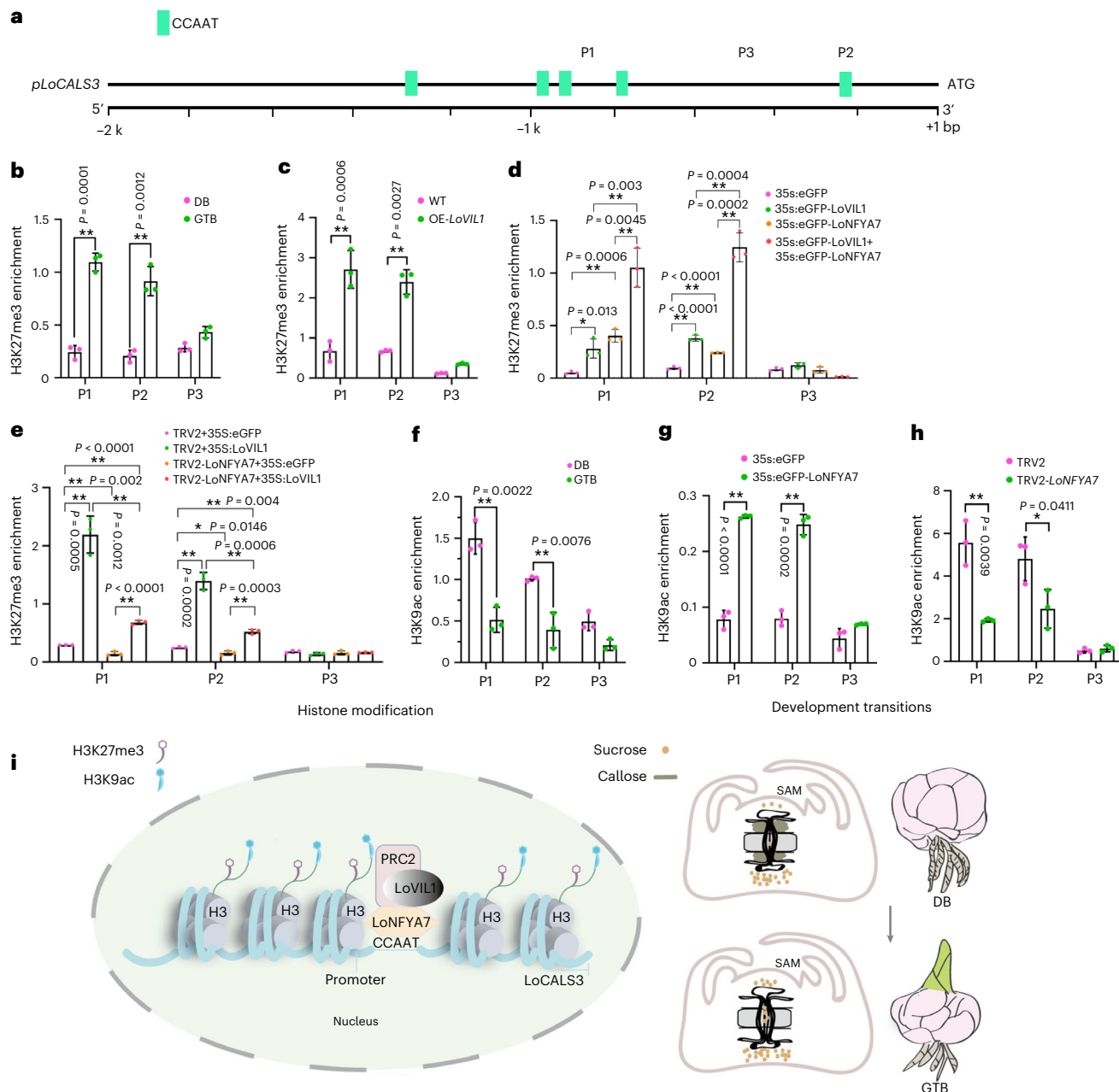


Fig. 6 | LoNFYA7 recruits LoVIL1-PRC2 to enhance H3K27me3 modification at *LoCALS3* locus. **a**, Schematic diagram of *LoCALS3* promoter regions tested for ChIP-qPCR, including P1 (-1175 bp to -915 bp; 3× CCAAT motif), P2 (-319 bp to -140 bp; 1× CCAAT motif) and P3 (-580 bp to -396 bp; without any CCAAT motif). Green boxes represent the CCAAT motif. **b–e**, H3K27me3 enrichment at the *LoCALS3* locus was assessed by ChIP-qPCR during bulb-growth transition (b), in *LoVIL1*-overexpressing lily (c), in dual-overexpressing SAMs (*LoVIL1* and *LoNFYA7*) (d), and in *LoNFYA7*-silenced and *LoVIL1*-overexpressing SAMs (e). Antibodies against the H3K27me3 and H3 were used for IP. Enriched values were normalized to the H3 level. Data in b–e represent mean ± s.d. of 3 biological replicates (two-sided Student's *t*-test). **f–h**, H3K9ac enrichment at *LoCALS3* locus using ChIP-qPCR during bulb-growth transition (f), in *LoNFYA7*-overexpressing SAMs (g) and in *TRV2-LoNFYA7* bulbs (h). Antibodies against H3K9ac and H3 were used for IP. Enriched values were normalized to the level of H3.

Data in f–h represent mean ± s.d. of 3 biological replicates (two-sided Student's *t*-test). **i**, Model depicting the epigenetic regulation of *LoCALS3* by *LoNFYA7* and *LoVIL1-PRC2* and its role in regulating bulb-growth transition in lily. In SAMs of DB (right images), PD are blocked by callose, restricting cellular communication and symplastic transport of sucrose. This is required to maintain bulb dormancy in lily. During bulb-growth transition (left images), *LoVIL1* is recruited by the *LoNFYA7* TF, which recognizes CCAAT motifs on the *LoCALS3* promoter. *LoVIL1-PRC2* represses *LoCALS3* transcription by enhancing H3K27me3 modification. This promotes cellular communication through PD and sugar symplastic transport in SAMs, activating cell activity and facilitating bulb-growth transition (right images). In addition, *LoNFYA7* may also play a role in H3K9ac regulation through an unknown mechanism, with H3K9ac potentially fine-tuning *LoNFYA7* transcription.

We first analysed central bud development after 8 weeks of cold storage to assess the speed of growth transition (Fig. 7h). Then we detected *LoVIL1* expression and compared it with central bud elongation (Fig. 7h). Surprisingly, *LoVIL1* was significantly correlated with central

bud elongation ($R^2 = 0.5912, P = 0.0433$, Pearson correlation) (Fig. 7i), showing that *LoVIL1* is a valid index for bud-growth transition in lily bulbs. Similarly, *LoCALS3* and *LoFT1* were also correlated with central bud development (Extended Data Fig. 10).

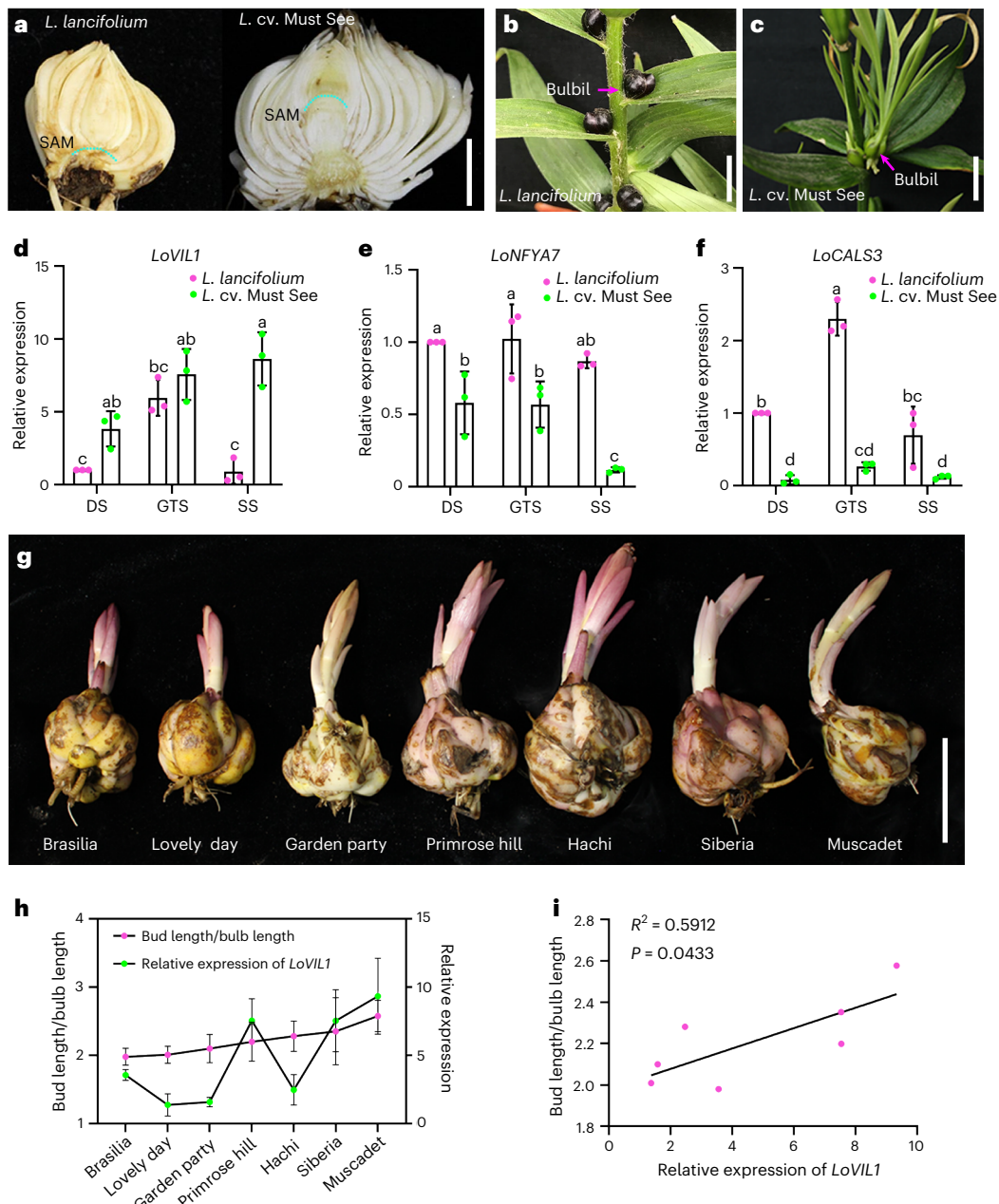


Fig. 7 | *LoVIL1* is a reliable index for growth-transition trait in lily bulbs.

a, Variation in growth-transition trait in bulbs between *L. lancifolium* (slow growth transition) and *L. cv. Must See* (fast growth transition). Images were taken when stems were completely withered aboveground in autumn and harvested simultaneously. The blue-green dotted line outlines the central bud. Scale bar, 5 cm. **b,c**, Consistency of growth-transition trait between bulblets and bulbs in *L. lancifolium* (**b**) and *L. cv. Must See* (**c**). Scale bars, 1 cm. **d–f**, Expression profiles of *LoVIL1* (**d**), *LoNFYA7* (**e**) and *LoCALS3* (**f**) in SAMs of bulbs at different stages. DS, dormant stage; GTS, growth-transited stage; SS, sprouting stage (12 °C treated 2 weeks after growth transition). Data in **d–f** represent mean \pm s.d. of 3 biological

replicates ($n = 3$ independent bulbs per replicate). Different letters above bars indicate significant differences ($P = 0.0025$ in **d**, $P = 0.0001$ in **e**, $P = 0.0001$ in **f**) determined using ANOVA with Turkey's HSD tests for pairwise comparisons.

g, Cultivars of Oriental lilies with varying growth-transition traits, ranging from slower to faster (left to right). Images were taken after 8 weeks of cold storage. Scale bar, 5 cm. **h**, Central bud development and *LoVIL1* expression in Oriental lilies 8 weeks after cold storage. Data are presented as mean \pm s.d. of 3 biological replicates ($n = 30$ bulbs per replicate for bud-growth analysis; $n = 3$ bulbs per replicate for expression analysis). **i**, Pearson correlation analysis of *LoVIL1* expression and central bud development.

In summary, *LoVIL1* is a good index for the growth transition following dormancy release and can be used for lily breeding.

Discussion

Regulation of PD transport during LTCT

Plants evolved unique cell-cell connections, the PD, during multicellularization, which enable long-distance and short-distance

communications and coordinate plant development and responses to various stresses³². PD create multiple routes for intercellular trafficking of a large spectrum of molecules, including RNAs (such as *FT* mRNA), proteins, hormones and metabolites (such as sugars)³³. By regulating cell-cell communication, PD control the switch from plant dormancy to sprouting. PD are blocked in dormant seeds (Crassulaceae family) and woody buds (Poplar), while they are open when dormancy

is released^{10,34}. Moreover, the high density of open PD contributes to dormancy release in potato aerial tubers¹¹. In this study, we demonstrated that closed PD led to bulb dormancy, while open PD enabled continuous growth in lily (Figs. 1e,g and 2g,h,j). Moreover, we identified a novel NF-YA member, LoNFYA7, which recruits the VIL1–PRC2 complex, enhances H3K27me3 at *LoCALS3* locus and fine-tunes *LoCALS3* expression during growth transition (Fig. 6i).

Callose deposition and degradation in PD control intercellular trafficking³² and are regulated by hormones and environmental cues. In poplar, (SD stimulate callose deposition in PD in buds by increasing endogenous ABA¹⁰. In contrast, cold acclimation during the winter increases endogenous GA, leading to callose degradation in PD, which promotes bud dormancy release¹². Apart from ABA and GA, cytokinins, auxin and salicylic acid control *CALS* expression and callose deposition^{4,12,35}. In *N. benthamiana*, PD transport is dynamically regulated by the circadian clock, such that knocking out of the core circadian clock gene, *LATE ELONGATED HYPOCOTYL/CIRCADIAN CLOCK ASSOCIATED 1* (*LHY/CCA1*), allows light to strongly promote PD transport during the subjective night³⁶. A recent study shows that *CCA1* and *LHY* contribute to the vernalization-triggered VIN3 induction at mild cold temperatures in *Arabidopsis*¹⁶. Here we demonstrate that *LoVIL1* is induced by LTCT and negatively regulates *LoCALS3* expression, contributing to recovering PD transport in dormant SAMs, hence to bud growth (Fig. 2). Our results provide a mechanism for how circadian genes regulate PD transport under LTCT/vernalization process. In dormant bulbs, abundant *LoCALS3* in SAMs and scale primordia induce PD closure and low intake of sugars, contributing to the maintenance of bulb dormancy (Fig. 3). During the growth transition, *LoVIL1* is stimulated in SAMs and scale primordia by LTCT, repressing *LoCALS3* and activating PD transport and intake of sugars (Fig. 2). Previously, *FT* mRNA and protein were shown to be transported to the SAM by phloem long-distance delivery and by PD, and to dilate PD microchannels during cell–cell trafficking, in agreement with *FT*'s role in bud dormancy in poplar and gentian^{12,37}. In this study, we found that *LoFT1* is increased in the SAM of growth-transited bulbs, *LoNFYA7*-silenced bulbs and *LoCALS3*-silenced bulbs but is decreased in *LoVIL1*-silenced bulbs. This suggests a positive role of *LoFT1* in PD transport and the bud-growth transition (Figs. 1j, 2m, 3j and 4o), although further studies are needed to support this function. Moreover, dilated PD also contributes to the growth transition by increasing symplastic transport (Fig. 1i), indicating that sugars are in high demand for cell division/differentiation in SAMs.

NF-YA7 recruits VIL1–PRC2 for H3K27me3 and growth transition

The evolutionarily conserved PRC2 complex modifies the structure and compaction of chromatin by adding H3K27me3 to target sites and repressing gene transcription, thereby controlling phase transitions and cell differentiation³⁸. The VIL1–PRC2 complex is composed of four core components: VIL1/VRN5, FIE, MSI1 and SWINGER (SWN), and is responsible for the vernalization process by repressing the FT repressor, FLC³⁸. However, the binding specificities of VIL1 are unknown^{19,39}. Recently, three TFs: BPCs, ARABIDOPSIS ZINC FINGER1 (AZF1) and TRBs, were proven to recruit PRC2 complex to target genes^{24,40}. Whether other TFs participate in PRC2 recruitment is still unknown. Here we bridge the gaps between VIL1 and target genes, showing that the NF-Y family member, LoNFYA7, is capable of recruiting the LoVIL1–PRC2 complex and targeting *LoCALS3* locus by recognizing the Cce (Fig. 5). During the growth transition, H3K27me3 was enhanced at *LoCALS3* locus, suggesting that other NF-YA members are possibly involved in this process (Fig. 6b). The LoVIL1–PRC2 complex increased the H3K27me3 levels at *LoCALS3* locus to promote intercellular communication and the growth transition (Figs. 2 and 6). Processes including bud growth, flower development and flowering time were all delayed after silencing of *LoVIL1* in bulbs (Fig. 2 and Extended Data Fig. 3). Therefore, there are common features between vernalization and the growth transition:

(1) LTCT plays positive roles in these two processes; (2) both processes are controlled by the PD dynamics that control cell–cell communications; (3) some genes act as the nexus in the growth transition and vernalization. Apart from the *FT* gene, the vernalization gene, *LoVIL1*, is also involved.

In this study, *LoVIL1* is presented as a potential marker for breeding lily cultivars with faster growth transition and early flowering traits (Fig. 7 and Extended Data Fig. 3). By comparing *VIL1* promoters in Must See and *L. lancifolium*, we find that there is a unique GA-response *cis*-element (CCTTTG)⁴¹ in Must See (Extended Data Fig. 8c), which may positively respond to GA during the growth transition by DNA binding with one finger (DOF) and DELLA proteins. However, the underlying mechanism needs further study. In addition, overexpression of *LoVIL1* not only generates evergrowing lily, but also changes leaf traits with early senescence, curly shape and abundant anthocyanin (Fig. 2g and Extended Data Fig. 4). H3K4me3 and H3K27me3 are reported to be involved in regulating anthocyanin biogenesis genes and *SENESTENCE-ASSOCIATED GENES* (*SAGs*) in *Arabidopsis* leaves, respectively^{42,43}. The curled leaf phenotype of OE-*LoVIL1* is similar to the *clf* mutant in *Arabidopsis*⁴⁴, suggesting that the PRC2 complex plays a role in leaf development.

NF-Y transcription factors are critical epigenetic mediators

NF-Y, also termed haem-activated protein or CCAAT binding factor, is a heterotrimeric TF comprising three distinct subunits: NF-YA, NF-YB and NF-YC, the latter two hosting histone-fold domains that allow them to form the heterodimer analogous to the dimer formed by histones H2B and H2A⁴⁵. NF-YA binds this heterodimer and provides sequence specificity for binding to the CCAAT box, which occurs in 30% of eukaryotic promoters and is crucial for promoter activity⁴⁵. In mammals, NF-Y has been shown to facilitate a permissive chromatin conformation and to be essential for the establishment of histone posttranslational modifications such as H3K4me3, H3K79me2 and H3K36me3, as well as some types of acetylation, but to be independent for posttranslational modifications including H3K27me3 and H3K9ac⁴⁶. However, our knowledge about NF-Y in plants is lagging. In plants, NF-Y TFs are critical for plant development and stress response including flowering time, photomorphogenesis, ABA-mediated seed germination and vernalization⁴⁷. During seed germination, NF-Y acts as an activator or repressor by modulating ABA and GA signalling pathways^{48,49}. Opposite to NFYA2/5/8/10 in *Arabidopsis*⁵⁰, we found that LoNFYA7 is a repressor of the growth transition in lily, as silencing of LoNFYA7 results in accelerated growth transition (Fig. 4j). Moreover, we found that LoNFYA7 participates in the growth transition by blocking PD and limiting cell–cell communication (Fig. 4l–o). Interestingly, although LoNFYA7 is involved in the growth transition in lily bulbs, it is not significantly related to the bud-growth-transition trait in various cultivars (Extended Data Fig. 10d), suggesting gene redundancy in the NF-Y family or the presence of alternative mechanisms.

The NF-Y family is reported to be involved in histone methylation and acetylation in plants. In *Arabidopsis*, NFYC9 is a key component controlling the flowering process by modulating H3K27me3 on flowering-related genes via direct interaction with RELATIVE OF EARLY FLOWERING 6 (REF6, an H3K27 demethylase) and CURLY LEAF (CLF, a PRC2 component)^{51,52}. NFYC3/4/9 can interact with HISTONE DEACETYLASE 15 (HDA15) and play roles in histone acetylation during hypocotyl elongation⁵³. Apart from NF-YCs, NF-YAs and NF-YBs are also capable of affecting H3K27me3 levels in flavonoid biosynthesis in tomatoes via unknown mechanisms⁵⁴. Here we showed that the NF-YA member, LoNFYA7 (1) interacts with the VIL1–PRC2 complex and enhances H3K27me3 at *LoCALS3* locus; (2) interacts with LoNFYC6, which is expressed during the growth transition but cannot interact with LoVIL1 (Extended Data Fig. 5); and (3) is involved in the crosstalk between H3K27me3 and H3K9ac, which may fine-tune *LoCALS3* expression during the growth transition (Fig. 6 and Extended Data Fig. 7). Previously in

soybeans, GmNFYA competitively interacted with GmMSI4 to remove HISTONE DEACETYLASE 13 (GmHDA13) function for maintenance of histone acetylation and activation of stress-responsive genes for salt tolerance³¹. In this study, after cold storage, the expression of *LoNFYA7* was decreased, accompanied by increased H3K27me3 levels at *LoCALS3* locus. This suggests that other NF-YAs or other TFs may collaborate to recruit VIL1–PRC2. Future studies should focus on understanding how NF-Y family members coordinately and individually participate in histone modifications during growth transition, as well as elucidating the mechanisms of VIL1–PRC2 recruitment by TFs.

Methods

Plant material and growth conditions

Lily cv. Siberia bulbs ($\phi = 4.6\text{--}5.1\text{ cm}$) were harvested early in May at Nanping City (118.17° N, 26.65° E), Fujian Province, or in October at Lingyuan City (119.40° N, 41.25° E), Liaoning Province. Bulbs were stored in a moist substrate (~30% humidity) with mixtures of peat and vermiculite (1:1 v/v) at 4 °C (cold treatment) in the dark. Then these bulbs were potted in the greenhouse at 24 °C and under long day (16/8 h light/dark) conditions. SAMs were collected from the bulbs at different stages, and the growth of the central bud was detected by longitudinal section. Six biological experiments were performed ($n = 5$ bulbs).

To test the effect of PD during the bud-growth transition in lily bulbs, axenic dormant Siberia bulbs ($\phi = 1\text{ cm}$) were cultivated on Murashige and Skoog (MS) medium containing 1 mM NEM, 1 mM BDM or 1 mM DDG. MS medium was used as the control. The germination rate was scored after 4 weeks. Germination was assessed when leaves developed on the scale. The experiment was performed three times with at least 20 bulbs for each sample.

RNA extraction and RT-qPCR

Total RNA was extracted from 100 mg of sample by using the RNA-easy isolation reagent (Vazyme) and RNase-free DNase I. Then 1.0 µg of total RNA was used to synthesize cDNA using the HiScript III 1st Strand cDNA synthesis kit (+gDNA wiper, Vazyme). RT-qPCRs were run using the Step One Plus real-time PCR system (Applied Biosystems) with the ChamQ Universal SYBR qPCR master mix (Vazyme). Reaction processes were as follows: 3 min at 95 °C, 42 cycles of PCR (10 s at 95 °C, 20 s at 60 °C and 20 s at 72 °C) and dissociation from 65 °C to 95 °C. The F-box family protein was used as the internal control for the normalization of gene expression⁵⁵. The data were analysed using the Data Processing System (v.9.01; Zhejiang University, Hangzhou, China). The primers used in this study are listed in Supplementary Table 1.

RNA-sequencing

Total RNA was extracted from bud samples from dormant bulbs (0 weeks of LTCT) and growth-transited bulbs (8 weeks of LTCT) using the RNAprep Pure Plant kit (Tiangen). Each stage contained three independent samples. RNA-sequencing was performed using the BGISEQ-500 platform at BGI. The fragment counts of each gene were normalized by fragments per kb per million. DEGs were analysed using the DESeq R package (1.10.1); GSEA was conducted using the clusterProfiler package in R (v.4.2.3) to determine whether genes belonging to a specific Gene Ontology term show significantly concordant differences.

Scanning electron microscopy

Central buds in lily bulbs were collected and fixed in FAA solution (50% ethanol, 5% acetic acid, 3.7% formaldehyde) for 8 h, under vacuum for 30 min. Treated buds were then dried by submersion with gentle agitation in an increasing gradient of ethanol (50%, 70% and 90% ethanol for 1 h, and two times in 100% ethanol for 1 h) at room temperature. The dried sample was placed on a scanning electron microscopy stub and their tiny scales were removed under the stereo microscope. Images were taken by using a Philips Quanta 200 FEI scanning electron microscopy.

Imaging callose at PD using aniline blue

To determine callose in the PD, the lily's central buds were isolated and fixed in 50 ml 95% ethanol to deactivate enzymes that can synthesize callose due to tissue manipulation. Rehydration buds were embedded in agar and sectioned with a vibratome. Callose in PD was observed and quantified by aniline blue staining as previously described⁵⁶. The fixed SAM was sectioned and stained with aniline blue and PD were quantified in the micrographs and normalized to 12 µm of the plasma membrane in each image. Three biological replicates were performed, with six samples per biological repeat.

PD TEM imaging and quantification

Lily SAMs from different treatments or stages were fixed with 2.5% (w/v) glutaraldehyde overnight at 4 °C. The samples were washed with 0.1 M phosphate buffer (pH 7.0) and post-fixed with 1% (w/v) osmium tetroxide. The permeation-treated samples were embedded with Spurr's embedding agent and heated at 70 °C overnight. Ultrathin sections of 70 nm thickness were obtained using a LEICA EM UC7 ultramicrotome and transferred onto 200-mesh formvar/carbon-coated nickel grids (Gilder). The samples were stained with saturated uranyl acetate and 0.2% (w/v) lead citrate at room temperature. The sections were visualized with a Hitachi H-7650 electron microscope. The length of cell walls was calculated using ImageJ/Fiji. At least three biological replicates were calculated.

CFDA labelling

To simulate symplastic transport in bulbs, application and visualization of the symplastic fluorescent dye CFDA were performed as previously described⁵⁷, with some modifications. CFDA (APExBIO, C4995) was prepared as a 50 mg l⁻¹ work solution in acetone. Direct loading of approximately 20 µl CFDA solution into the wedge-shaped block in the upper part of the abaxial surface of the outer bulb scales was performed to expose the vascular bundle. The loading site was immediately fixed with polythene film and aluminum foil. The CFDA-fed materials were incubated back to the original growth condition to allow for CF transport for at least 3 h before monitoring. A frozen slicer (Leica CM1850) was used to slice the explants into 60-µm-thin sections, after which a fluorescence microscope (Zeiss LSM-880) was used to monitor the movement of the CF fluorescence under blue light (488 nm).

RNA *in situ* hybridization

RNA *in situ* hybridization and image acquisition were performed as previously described⁵⁸, with minor modifications. SAMs of DB (0 weeks of LTCT) and GTB (8 weeks of LTCT) were fixed with formaldehyde-acetic acid-ethanol and embedded with paraffin. Then, sections (10 µm thickness) were obtained with an auto rotary microtome (149AUTO00C1, Leica) and transferred on polylysine-coated slides (Fisher). *In situ* probes were synthesized with a DIG RNA labelling kit (Roche) by PCR amplification with gene-specific primers containing T7 and SP6 RNA polymerase binding sites.

Virus-induced gene silencing

VIGS was performed as previously described^{59,60}, with minor revision. A gene-specific fragment (300 bp in length) of *LoVIL1*, *LoNFYA7* or *LoCALS3* was used to construct pTRV2-*LoVIL1*, pTRV2-*LoNFYA7* or pTRV2-*LoCALS3*, respectively. Vectors including pTRV1, pTRV2 and reconstructed pTRV2 were individually transformed into *Agrobacterium tumefaciens* strain EHA105. Transformed agrobacteria were grown in liquid Luria-Bertani medium with 50 mg l⁻¹ kanamycin and 25 mg l⁻¹ rifampicin at 28 °C, and were harvested by centrifugation. Pellets were resuspended in infiltration buffer (10 mM MgCl₂, 200 µM acetosyringone and 10 mM MES; pH 5.8) to the final concentration (optical density (OD)₆₀₀ = 1.0). A mixture of *A. tumefaciens* cultures contained pTRV1 and pTRV2-*LoVIL1* (pTRV2-*LoNFYA* or pTRV2-*LoCALS3*) at a 1:1 (v/v) ratio. The mixture of pTRV1 and pTRV2 was used as the control. Mixtures were placed in the dark at room temperature for

3 h before agroinfiltration. Lily bulbs pinned with five holes around the base plates were submerged into the mixtures and vacuumed at -25 kPa for 15 min. The infiltrated bulbs were dried overnight and stored in moist peat moss (-30% humidity) at 4°C before potting. At least 20 bulbs were used for each sample. Bulbs of *L. lancifolium* were agroinfiltrated in the same way and stored in moist peat moss at room temperature for 14 weeks ($n = 20$ bulbs per sample). Three biological repeats were performed.

Generation of transgenic lily

To generate the *LoVIL1*-overexpressing lily, *35S:eGFP-LoVIL1* was inserted into the pCAMBIA2300 vector. Transgenic plants were selected on half MS media with 150 mg l^{-1} kanamycin via agroinfiltrated discs according to previously described protocol⁶¹. Transformed plants were validated by western blot and RT-qPCR.

To test the effect of NEM on transgenic lilies, bulbs of OE-*LoVIL1* lines (#1, #3 and #4) were grown on MS or MS containing 1 mM NEM and placed in a growth chamber at 24°C under 16/8 h light/dark conditions for 4 weeks.

Transient overexpression in lily calluses and bulbs

Genes were inserted into pCAMBIA2300 vectors and further used for transient overexpression. The empty pCAMBIA2300 vector was used as the control. Embryonic lily calluses were induced with filaments on MS medium containing 0.1 mg l^{-1} -naphthalacetic acid and 0.3 mg l^{-1} picloram. The calluses ($0.5\text{ cm} \times 0.5\text{ cm}$ in size) were submerged in 20 ml agroinfiltration solution (10 mM MgCl_2 , $200\text{ }\mu\text{M}$ acetosyringone and 10 mM MES ; pH 5.8; OD₆₀₀ = 0.1) in a 50 ml syringe and exposed to a negative pressure by pulling the plunger to the dosage line at 40 ml for 1 min. Then, calluses were dried on axenic absorbent paper to remove the solution and co-cultured on MS medium containing 200 mM acetosyringone, 0.1 mg l^{-1} -naphthalacetic acid and 0.3 mg l^{-1} picloram in the dark for 72 h.

Lily bulbs punctured with five holes on the basal plate were submerged into the agroinfiltration mixtures and vacuumed at -25 kPa for 15 min. The infiltrated bulbs were dried overnight and soaked in a moist substrate at room temperature for 3 d. At least 10 bulbs were used for each sample and three biological repeats were tested.

In planta histone methylation assay

The change in H3K27me3 activity caused by *LoVIL1* was tested in planta. *N. benthamiana* plants were transiently transformed by agroinfiltration with the *35S:eGFP-LoVIL1* construct to overexpress *LoVIL1* proteins and grown in the dark for 3 d before nuclei isolation. *35S:eGFP* was used as the control. Isolated nuclei were visualized by DAPI staining (blue) and incubated with the first antibody overnight (anti-H3K27me3; Beyotime; dilution 1:1,000). Alexa Fluor 555 goat anti-rabbit was used as the second antibody (Invitrogen). The fluorescence signals (excitation wavelengths: 405 nm, 488 nm, 561 nm) were collected on a fluorescence microscope (Zeiss LSM-880). The fluorescence intensity of immuno-labeled nuclei was quantified using ImageJ (v.1.53c). Four biological repeats were performed and 10 nuclei per repeat were measured.

Y2H assays

For library screening, the coding sequence of *LoVIL1* were inserted into the pGBT7 vector and transformed into the AH109 yeast strain as the bait. The cDNA library of dormant lily bulbs was transformed into the Y187 yeast strain. The bait was mated with the prey library via growing at 30°C overnight in 50 ml of 2xYPDA (yeast extract, peptone, dextrose and adenine) broth. The mated yeasts were able to grow on SD-/Leu-/Trp (SD-LT) plates. The interacting partners were screened on SD-/Leu-/Trp-/His (SD-LTH) plates after 3 d.

To test the interaction between *LoVIL1* and *LoNFYA7*, pGADT7-*LoNFYA7* and pGBT7-*LoVIL1* vectors were co-transformed into the AH109 yeast strain. To test the interaction between *LoVIL1* and *LoMSI1*, pGADT7-*LoVIL1* and pGBT7-*LoMSI1* vectors were

co-transformed into the AH109 yeast strain. The interaction was validated by yeast grown on the SD-LTH plate. The transformant of pGADT7 and pGBT7 was used as the negative control, while the transformant of AD-T7 and BD-53 was used as the positive control.

Split-luciferase assay

Open reading frames (ORFs) of *LoVIL1* and *LoNFYA7* were cloned in-frame with those of cLUC and nLUC, respectively⁶². The fusion vectors were then transformed into *Agrobacterium* strain EHA105 for transient over-expression in *N. benthamiana* leaves. Agrobacteria was resuspended in the infiltration buffer (10 mM MgCl_2 , $200\text{ }\mu\text{M}$ acetosyringone and 10 mM MES ; pH 5.8; OD₆₀₀ = 0.8). A mixture of *A. tumefaciens* cultures contained *LoVIL1* and *LoNFYA7* at a 1:1 (v/v) ratio. The mixture of cLUC and nLUC was used as the control. The luciferase was activated by luciferin solution (0.1% Triton X-100, 1 mM luciferin) after 3 d of infiltration and detected under a CCD camera (CHEMIPROHT 1300B/LND, 16 bits, Roper Scientific). The combination of cLUC+nLUC was used as the control. The interaction was confirmed in at least three biological replicates.

BiFC

LoVIL1 and *LoNFYA7* were cloned in-frame with N-terminal of yellow fluorescent protein (nYFP) and C-terminal of yellow fluorescent protein (cYFP), respectively⁶³. The BiFC plasmids were introduced into *Agrobacterium* strain GV3101 for transient transformation in *N. benthamiana* leaves. The infiltration buffer and operating procedures were the same as in the split-luciferase assay. The combination of nYFP+cYFP and protein fused with half YFP+the other half YFP were used as negative controls. The fluorescence signals of YFP and mCherry (the nuclear marker, ATRPL24B-mCherry, AT3G53020) were assessed by confocal microscopy (Zeiss LSM-880) with a 488 nm excitation laser and a 529–550 nm bandpass filter for YFP emission (green channel), and a 561 nm excitation laser and a 605–630 high-pass filter for mCherry emission (mCherry channel).

FRET assay

FRET experiments were conducted as described previously, with minor modifications⁶⁴. *LoVIL1* with His tag and *LoNFYA7* with GST tag were generated with pET28a and pGEX-4T vectors, respectively. *Escherichia coli* BL21 (DE3) cells were used for protein purification. A FRET assay was performed using the Add&Read anti-GST-Eu and Add&Read anti-6His-A2 regents (Vazyme) according to manufacturer instructions. An F-4500 fluorescence spectrometer (Tecan 4600) was used to detect values under OD₆₆₅ and OD₆₂₀.

Yeast 1-hybrid assay

The ORF of *LoNFYA7* was cloned into the prey vector (pGADT7), and oligonucleotides of *LoNFYA7*-binding sites were synthesized and ligated into the pAbAi vectors (Clontech). The linearized pAbAi vectors were transformed into the yeast strain Y1H Gold according to manufacturer instructions and selected on synthetic dropout medium/-uracil (SD/-U) plates with AbA^r. Then, pGADT7-*LoNFYA7* was transformed into the Y1H Gold strain harbouring *LoCALS3* promoter and selected by AbA^r on synthetic dropout medium/-uracil-leucine (SD/-UL) medium, and the empty pGADT7 was used as the negative control.

EMSA

Purified GST-tagged *LoVIL1* (mentioned above) was used in this assay. Hot probes harbouring *cis*-elements were synthesized and labelled with biotin. The recombinant protein was purified with maltose. EMSA was performed using the Light Shift Chemiluminescent EMSA kit (Thermo Fisher) according to manufacturer instructions.

Dual-luciferase transient expression assay

LoNFYA7, *LoVIL1* and enhanced green fluorescent protein (eGFP) were cloned into pGreenII 62-SK vectors. The *LoCALS3* promoter (~1,301 bp

to \sim 201 bp) was cloned into pGreenII 0800-LUC vector. The constructed vectors were transiently transferred into lily embryonic calluses by agroinfiltration as described above. Images of LUC signals were captured by the CCD camera. The activities of LUC and REN luciferases were measured using the Dual-LUC assay kit (Promega). Three biological repeats were used for each sample.

ChIP-qPCR

ChIP experiments were conducted as described previously, with minor modifications⁶⁵. Briefly, infected SAMs or calluses (3 g) were collected and ground into a fine powder in liquid nitrogen, and then homogenized well with 36 ml extraction buffer (0.4 M sucrose, 10 mM Tris-HCl (pH 8.0), 1 mM MgCl₂, 1 mM CaCl₂, 0.5% PVP40, 0.1 M PMSF, 1% (v/v) Triton X-100, 1 mM DTT). Then, 37% (v/v) formaldehyde was added immediately to the homogenized buffer until the final concentration was 1%. The mixed buffer was crosslinked on a shaker for 15 min at 4 °C and the reaction was stopped with 2 M glycine. Chromatin was isolated and sheared into fragments of 700–1,000 bp size by sonication. The sonicated chromatin was incubated with 10 µl antibody (H3, H3K9ac or H3K27me3; dilution 1:1,000) overnight at 4 °C. The treated chromatin was washed in order with low-salt, high-salt and TE buffers. The DNA–protein complex was eluted and reverse crosslinked at 65 °C overnight. DNA was purified using the QIAquick PCR purification kit (Qiagen) and subsequently used for qPCR analysis. The results were calculated as the percentage of input DNA according to the Champion ChIP–qPCR user manual (SABioscience). Three biological replicates were performed in this assay.

Subcellular localization

The ORF of *LoVIL1* was cloned into the pCAMBIA2300 vector to fuse in-frame with eGFP. The reconstructed vector and nuclear marker (ATRPL24B-mCherry) were introduced into *A. tumefaciens* strain EHA105 and transiently overexpressed in *N. benthamiana* leaves. Fluorescence signals were assessed using a Zeiss LSM-880 confocal microscope with 488 nm/515–535 nm GFP excitation/emission (green channel) and 561 nm/605–630 nm mCherry emission excitation/emission (mCherry channel). Subcellular localization was confirmed by at least three biological repeats.

Statistical analysis

Statistical analyses were performed using one-way analysis of variance (ANOVA) followed by Tukey's honestly significant difference (HSD) tests for pairwise comparisons, and Student's *t*-test. GraphPad Prism (v.8.0.2) and DPS Statistics (v.9.01) were used for analysis.

Reporting summary

Further information on research design is available in the Nature Portfolio Reporting Summary linked to this article.

Data availability

Data supporting the findings of this study are available from the corresponding author upon request. All primers used in this study are listed in Supplementary Table 1. RNA-sequencing data that support the findings of this study have been deposited in the NCBI Bioproject database under accession number PRJNA935924. Information on related genes in this study has been uploaded to GenBank in the NCBI Nucleotide database, including *LoVIL1* (OQ469822), *LoNFYAT* (OQ469823), *LoCALS3* (OQ469824), *LoFT1* (OQ469825), *LoCALS5* (OQ469826), *LoCALS7* (OQ469827), *LoCALS10* (OQ469828), *LoCALS12* (OQ469829) and *LoHDA14* (OQ857021). Source data are provided with this paper.

References

- Pan, W. et al. ABA and bud dormancy in perennials: current knowledge and future perspective. *Genes* **12**, 1635 (2021).
- Wu, J. et al. GhTCP19 transcription factor regulates corm dormancy release by repressing GhNCED expression in *Gladiolus*. *Plant Cell Physiol.* **60**, 52–62 (2019).
- Bohlenius, H. et al. CO/FT regulatory module controls timing of flowering and seasonal growth cessation in trees. *Science* **312**, 1040–1043 (2006).
- Singh, R. K., Miskolczi, P., Maurya, J. P. & Bhalerao, R. P. A tree ortholog of SHORT VEGETATIVE PHASE floral repressor mediates photoperiodic control of bud dormancy. *Curr. Biol.* **29**, 128–133 (2019).
- Azeel, A., Miskolczi, P., Tylewicz, S. & Bhalerao, R. P. A tree ortholog of APETALA1 mediates photoperiodic control of seasonal growth. *Curr. Biol.* **24**, 717–724 (2014).
- Ginzburg, C. Metabolic changes in *Gladiolus* cormels during the break of dormancy—the role of dark CO₂ fixation. *Plant Physiol.* **68**, 1105–1109 (1981).
- Wu, J. et al. *Gladiolus hybridus* ABSCISIC ACID INSENSITIVE 5 (GhABI5) is an important transcription factor in ABA signaling that can enhance *Gladiolus* corm dormancy and *Arabidopsis* seed dormancy. *Front. Plant Sci.* **6**, 960 (2015).
- Azeel, A. et al. EARLY BUD-BREAK 1 and EARLY BUD-BREAK 3 control resumption of poplar growth after winter dormancy. *Nat. Commun.* **12**, 1123 (2021).
- Leida, C., Conesa, A., Llacer, G., Badenes, M. L. & Rios, G. Histone modifications and expression of DAM6 gene in peach are modulated during bud dormancy release in a cultivar-dependent manner. *New Phytol.* **193**, 67–80 (2012).
- Tylewicz, S. et al. Photoperiodic control of seasonal growth is mediated by ABA acting on cell–cell communication. *Science* **360**, 212–215 (2018).
- Nicolas, M. et al. Spatial control of potato tuberization by the TCP transcription factor BRANCHED1b. *Nat. Plants* **8**, 281–294 (2022).
- Rinne, P. L. et al. Chilling of dormant buds hyperinduces FLOWERING LOCUS T and recruits GA-inducible 1,3-beta-glucanases to reopen signal conduits and release dormancy in *Populus*. *Plant Cell* **23**, 130–146 (2011).
- Sung, S. & Amasino, R. M. Vernalization in *Arabidopsis thaliana* is mediated by the PHD finger protein VIN3. *Nature* **427**, 159–164 (2004).
- Kim, D. H. & Sung, S. The binding specificity of the PHD-finger domain of VIN3 moderates vernalization response. *Plant Physiol.* **173**, 1258–1268 (2017).
- Zhao, Y., Antoniou-Kourounioti, R. L., Calder, G., Dean, C. & Howard, M. Temperature-dependent growth contributes to long-term cold sensing. *Nature* **583**, 825–829 (2020).
- Kyung, J. et al. The two clock proteins CCA1 and LHY activate VIN3 transcription during vernalization through the vernalization-responsive cis-element. *Plant Cell* **34**, 1020–1037 (2022).
- Kim, D. H., Zografos, B. R. & Sung, S. B. Vernalization-mediated VIN3 induction overcomes the LIKE-HETEROCHROMATIN PROTEIN1/POLYCOMB REPRESSION COMPLEX2-mediated epigenetic repression. *Plant Physiol.* **154**, 949–957 (2010).
- Kim, J. et al. Warm temperature-triggered developmental reprogramming requires VIL1-mediated genome-wide H3K27me3 accumulation in *Arabidopsis*. *Development* **150**, dev201343 (2023).
- Zong, W., Kim, J., Bordiyya, Y., Qiao, H. & Sung, S. Abscisic acid negatively regulates the Polycomb-mediated H3K27me3 through the PHD-finger protein, VIL1. *New Phytol.* **235**, 1057–1069 (2022).
- Bond, D. M., Wilson, I. W., Dennis, E. S., Pogson, B. J. & Jean Finnegan, E. VERNALIZATION INSENSITIVE 3 (VIN3) is required for the response of *Arabidopsis thaliana* seedlings exposed to low oxygen conditions. *Plant J.* **59**, 576–587 (2009).

21. Zhang, X. et al. Replication protein RPA2A regulates floral transition by cooperating with PRC2 in *Arabidopsis*. *New Phytol.* **235**, 2439–2453 (2022).
22. Sung, S., Schmitz, R. J. & Amasino, R. M. A PHD finger protein involved in both the vernalization and photoperiod pathways in *Arabidopsis*. *Genes Dev.* **20**, 3244–3248 (2006).
23. Kim, J. et al. Phytochrome B triggers light-dependent chromatin remodelling through the PRC2-associated PHD finger protein VIL1. *Nat. Plants* **7**, 1213–1219 (2021).
24. Xiao, J. et al. *Cis* and *trans* determinants of epigenetic silencing by polycomb repressive complex 2 in *Arabidopsis*. *Nat. Genet.* **49**, 1546–1552 (2017).
25. Wu, J. et al. Spatiotemporal restriction of FUSCA3 expression by class I BPCs promotes ovule development and coordinates embryo and endosperm growth. *Plant Cell* **32**, 1886–1904 (2020).
26. Sun, X. et al. Transcriptomics and targeted metabolomics reveal the regulatory network of *Lilium davidii* var. *unicolor* during bulb dormancy release. *Planta* **254**, 59 (2021).
27. Zhou, Y., Wang, W., Yang, L., Su, X. & He, M. Identification and expression analysis of microRNAs in response to dormancy release during cold storage of *Lilium pumilum* bulbs. *J. Plant Growth Regul.* **40**, 388–404 (2020).
28. Radford, J. E. & White, R. G. Inhibitors of myosin, but not actin, alter transport through *Tradescantia* plasmodesmata. *Protoplasma* **248**, 205–216 (2011).
29. Liu, L. & Chen, X. Intercellular and systemic trafficking of RNAs in plants. *Nat. Plants* **4**, 869–878 (2018).
30. Andres, F. & Coupland, G. The genetic basis of flowering responses to seasonal cues. *Nat. Rev. Genet.* **13**, 627–639 (2012).
31. Lu, L. et al. Nuclear factor Y subunit GmNFY α competes with GmHDA13 for interaction with GmFVE to positively regulate salt tolerance in soybean. *Plant Biotechnol. J.* **19**, 2362–2379 (2021).
32. Sankoh, A. F. & Burch-Smith, T. M. Approaches for investigating plasmodesmata and effective communication. *Curr. Opin. Plant Biol.* **64**, 102143 (2021).
33. Li, Z. P., Paterlini, A., Glavier, M. & Bayer, E. M. Intercellular trafficking via plasmodesmata: molecular layers of complexity. *Cell. Mol. Life Sci.* **78**, 799–816 (2021).
34. Kozieradzka-Kiszkurno, M. & Plachno, B. J. Are there symplastic connections between the endosperm and embryo in some angiosperms?—a lesson from the Crassulaceae family. *Protoplasma* **249**, 1081–1089 (2012).
35. Alazem, M., He, M. H., Moffett, P. & Lin, N. S. Abscisic acid induces resistance against bamboo mosaic virus through argonaute2 and 3. *Plant Physiol.* **174**, 339–355 (2017).
36. Brunkard, J. O. & Zambryski, P. Plant cell-cell transport via plasmodesmata is regulated by light and the circadian clock. *Plant Physiol.* **181**, 1459–1467 (2019).
37. Takahashi, H., Nishihara, M., Yoshida, C. & Itoh, K. Gentian FLOWERING LOCUS T orthologs regulate phase transitions: floral induction and endodormancy release. *Plant Physiol.* **188**, 1887–1899 (2022).
38. Forderer, A., Zhou, Y. & Turck, F. The age of multiplexity: recruitment and interactions of Polycomb complexes in plants. *Curr. Opin. Plant Biol.* **29**, 169–178 (2016).
39. De Lucia, F., Crevillen, P., Jones, A. M., Greb, T. & Dean, C. A PHD-polycomb repressive complex 2 triggers the epigenetic silencing of FLC during vernalization. *Proc. Natl. Acad. Sci. USA* **105**, 16831–16836 (2008).
40. Zhou, Y. et al. Telobox motifs recruit CLF/SWN-PRC2 for H3K27me3 deposition via TRB factors in *Arabidopsis*. *Nat. Genet.* **50**, 638–644 (2018).
41. Gubler, F. & Jacobsen, J. V. Gibberellin-responsive elements in the promoter of a barley high- pI a-amylase gene. *Plant Cell* **4**, 1435–1441 (1992).
42. Cai, H. et al. Epigenetic regulation of anthocyanin biosynthesis by an antagonistic interaction between H2A.Z and H3K4me3. *New Phytol.* **221**, 295–308 (2019).
43. Liu, C. et al. Polycomb repressive complex 2 attenuates ABA-induced senescence in *Arabidopsis*. *Plant J.* **97**, 368–377 (2019).
44. Re, D. A. et al. CURLY LEAF regulates microRNA activity by controlling ARGONAUTE 1 degradation in plants. *Mol. Plant* **13**, 72–87 (2020).
45. Nardini, M. et al. Sequence-specific transcription factor NF-Y displays histone-like DNA binding and H2B-like ubiquitination. *Cell* **152**, 132–143 (2013).
46. Dolfini, D., Gatta, R. & Mantovani, R. NF-Y and the transcriptional activation of CCAAT promoters. *Crit. Rev. Biochem. Mol. Biol.* **47**, 29–49 (2012).
47. Myers, Z. A. & Holt, B. F. III NUCLEAR FACTOR-Y: still complex after all these years? *Curr. Opin. Plant Biol.* **45**, 96–102 (2018).
48. Finkelstein, R., Reeves, W., Ariizumi, T. & Steber, C. Molecular aspects of seed dormancy. *Annu. Rev. Plant Biol.* **59**, 387–415 (2008).
49. Xu, L. et al. The NF-YC-RGL2 module integrates GA and ABA signalling to regulate seed germination in *Arabidopsis*. *Nat. Commun.* **7**, 12768 (2016).
50. Mu, J., Tan, H., Hong, S., Liang, Y. & Zuo, J. *Arabidopsis* transcription factor genes NF-YA1, 5, 6, and 9 play redundant roles in male gametogenesis, embryogenesis, and seed development. *Mol. Plant* **6**, 188–201 (2013).
51. Hou, X. et al. Nuclear factor Y-mediated H3K27me3 demethylation of the SOC1 locus orchestrates flowering responses of *Arabidopsis*. *Nat. Commun.* **5**, 4601 (2014).
52. Liu, X. et al. Temporal-specific interaction of NF-YC and CURLY LEAF during the floral transition regulates flowering. *Plant Physiol.* **177**, 105–114 (2018).
53. Tang, Y. et al. *Arabidopsis* NF-YCs mediate the light-controlled hypocotyl elongation via modulating histone acetylation. *Mol. Plant* **10**, 260–273 (2017).
54. Wang, J. et al. NF-Y plays essential roles in flavonoid biosynthesis by modulating histone modifications in tomato. *New Phytol.* **229**, 3237–3252 (2021).
55. Li, X. et al. Validation of reference genes for accurate normalization of gene expression in *Lilium davidii* var. *unicolor* for real-time quantitative PCR. *PLoS ONE* **10**, e0141323 (2015).
56. Zavaliev, R. & Epel, B. L. Imaging callose at plasmodesmata using aniline blue: quantitative confocal microscopy. *Methods Mol. Biol.* **1217**, 105–119 (2015).
57. Ruan, Y.-L. & Patrick, J. W. The cellular pathway of postphloem sugar transport in developing tomato fruit. *Planta* **196**, 434–444 (1995).
58. Zhang, X. et al. Transcription repressor HANABA TARANU controls flower development by integrating the actions of multiple hormones, floral organ specification genes, and GATA3 family genes in *Arabidopsis*. *Plant Cell* **25**, 83–101 (2013).
59. Tian, J. et al. TRV-GFP: a modified tobacco rattle virus vector for efficient and visualizable analysis of gene function. *J. Exp. Bot.* **65**, 311–322 (2014).
60. Wu, Z., Li, T., Cao, X., Zhang, D. & Teng, N. Lily WRKY factor LIWRKY22 promotes thermotolerance through autoactivation and activation of LDREB2B. *Hortic. Res.* **9**, uhac186 (2022).
61. Núñez de Cáceres, F. F., Davey, M. R. & Wilson, Z. A. A rapid and efficient Agrobacterium-mediated transformation protocol for *Lilium*. *Acta Hortic.* **900**, 161–167 (2010).
62. Chen, H. et al. Firefly luciferase complementation imaging assay for protein–protein interactions in plants. *Plant Physiol.* **146**, 368–376 (2008).

63. Waadt, R. et al. Multicolor bimolecular fluorescence complementation reveals simultaneous formation of alternative CBL/CIPK complexes in planta. *Plant J.* **56**, 505–516 (2008).
64. Yu, Y. et al. Arabidopsis REM16 acts as a B3 domain transcription factor to promote flowering time via directly binding to the promoters of SOC1 and FT. *Plant J.* **103**, 1386–1398 (2020).
65. Saleh, A., Alvarez-Venegas, R. & Avramova, Z. An efficient chromatin immunoprecipitation (ChIP) protocol for studying histone modifications in *Arabidopsis* plants. *Nat. Protoc.* **3**, 1018–1025 (2008).

Acknowledgements

This work was funded by the Beijing Natural Science Foundation (6212012 to J.W.), National Natural Science Foundation projects (grants 32172617 and 31701952 to J.W.), Research Outstanding Talents Training Project of the Ministry of Agriculture and Rural Affairs, Construction of Beijing Science and Technology Innovation and Service Capacity in Top Subjects (CEFF-PXM 2019_014207_000032), the 2115 Talent Development Program of China Agricultural University, the Project supported by the Strategic Development Department of China Association for Science and Technology, and 111 Project of the Ministry of Education (B17043).

Author contributions

J.W. and M.Y. designed the research. W.P. and J.L. cloned constructs and performed most of the experiments and data analysis. Y.Z., Y.X., C.L. and S.W. helped perform RT-qPCR and lily transformation assays. W.P., J.L., M.Y. and J.W. conceived the research and designed the experiments. Y.D., Z.L., S.F., Y.Y. and X.Z. provided lily species and bulbs. W.P. and J.W. wrote the original paper. J.W., M.Z. and S.G. revised the paper. J.W. agreed to serve as the corresponding author and ensure communication.

Competing interests

The authors declare no competing interests.

Additional information

Extended data is available for this paper at <https://doi.org/10.1038/s41477-023-01492-z>.

Supplementary information The online version contains supplementary material available at <https://doi.org/10.1038/s41477-023-01492-z>.

Correspondence and requests for materials should be addressed to Jian Wu.

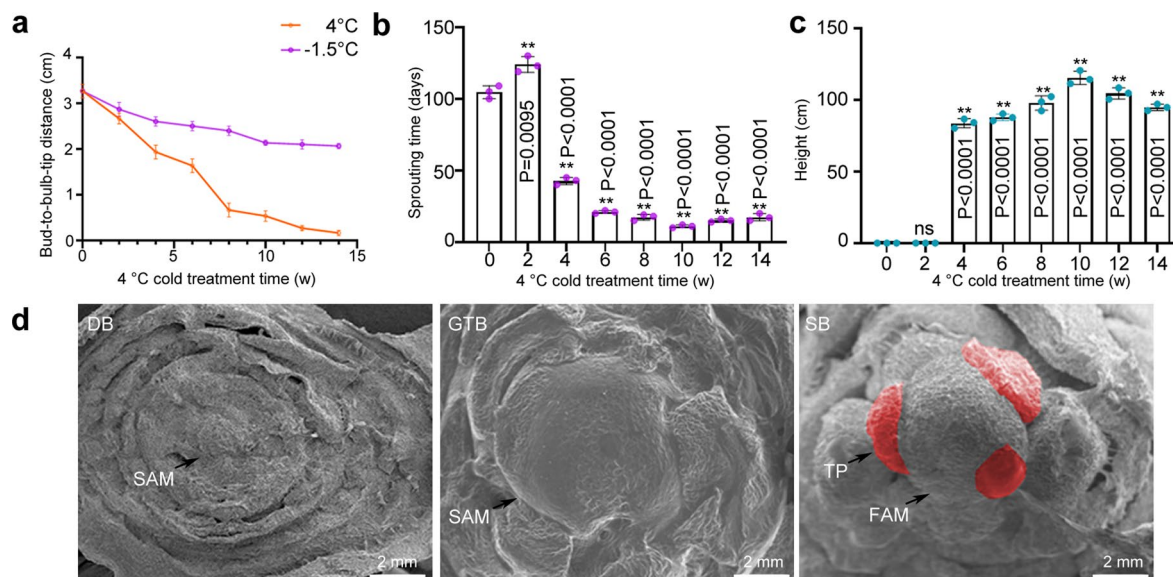
Peer review information *Nature Plants* thanks Steve van Nocker and the other, anonymous, reviewer(s) for their contribution to the peer review of this work.

Reprints and permissions information is available at www.nature.com/reprints.

Publisher's note Springer Nature remains neutral with regard to jurisdictional claims in published maps and institutional affiliations.

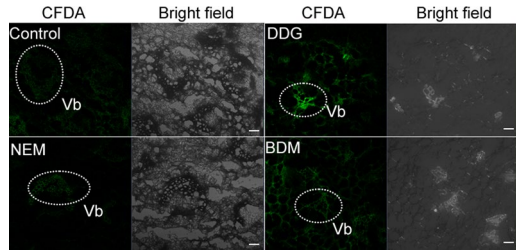
Springer Nature or its licensor (e.g. a society or other partner) holds exclusive rights to this article under a publishing agreement with the author(s) or other rightsholder(s); author self-archiving of the accepted manuscript version of this article is solely governed by the terms of such publishing agreement and applicable law.

© The Author(s), under exclusive licence to Springer Nature Limited 2023



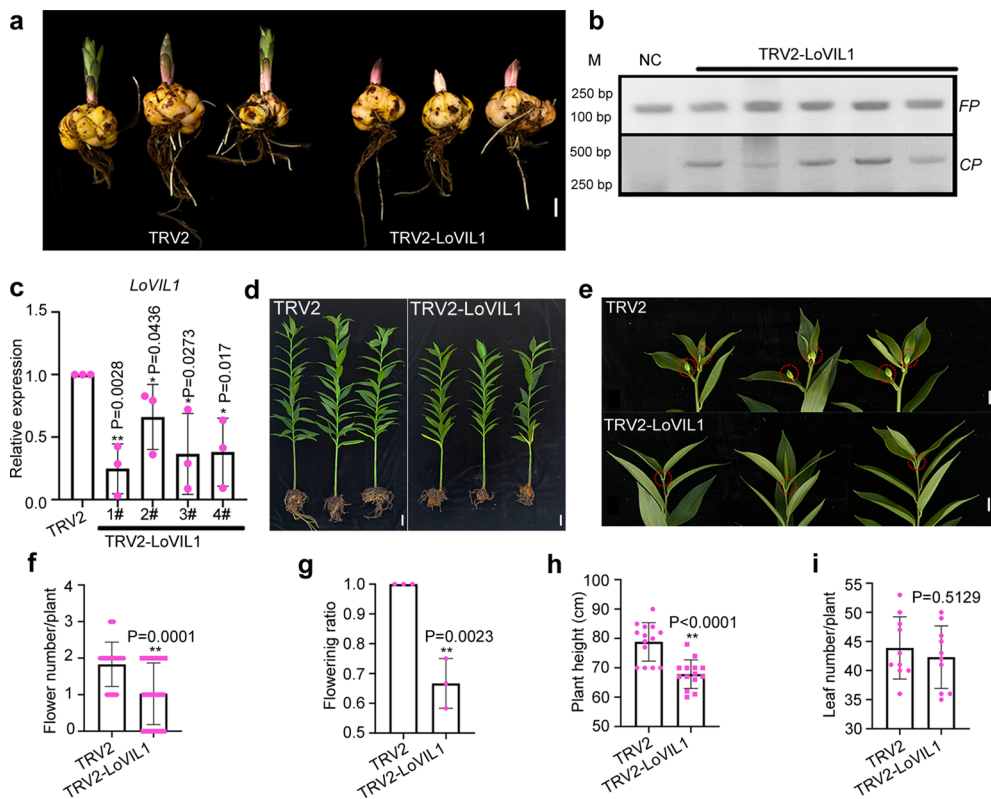
Extended Data Fig. 1 | Effect of cold storage duration on lily sprouting and flower differentiation. **a**, Bulb growth transition: cold storage (4 °C) accelerates bulb growth transition, while frozen storage (-1.5 °C) delays it for long-term storage. The distance between the bud and the bulb tip shows the bud elongation during storage. Data are presented as mean ± s.d. of three biological replicates (n = 5 bulbs per replicate). **b**, Bulb sprouting: effect of cold storage (4 °C) duration on bulb sprouting. Data are presented as mean ± s.d. of three biological replicates (n = 100 bulbs per sample; two-sided Student's *t*-test). **c**, Plant height: effect of cold storage (4 °C) duration on plant height 90 days after planting. Data are presented as mean ± s.d. of three biological replicates (n = 100 bulbs per sample; two-sided Student's *t*-test; ns: not significant and *p* > 0.05).

d, Central bud development: central bud development at different stages using scanning electron microscopy. In DBs, the central bud was flat on the basal plate. In GTBs, the central bud grew up to $\frac{2}{3}$ bulb height and the SAM was evident. After sprouting, the SAM of the central bud was converted into FAM. The highlighted area in red indicates the tepal primordium. Consistent results were obtained in at least three independent bulbs. DB: dormant bulbs (cold storage at 4 °C for 0 weeks); GTB: growth transited bulbs (cold storage at 4 °C for 8 weeks); FAM: flower apical meristem; SAM: shoot apical meristem; SB: sprouting bulbs (cold storage at 4 °C for 8 weeks and then sprouting at 12 °C for 2 weeks); TP: Tepal primordium. Scale bar, 2 mm.



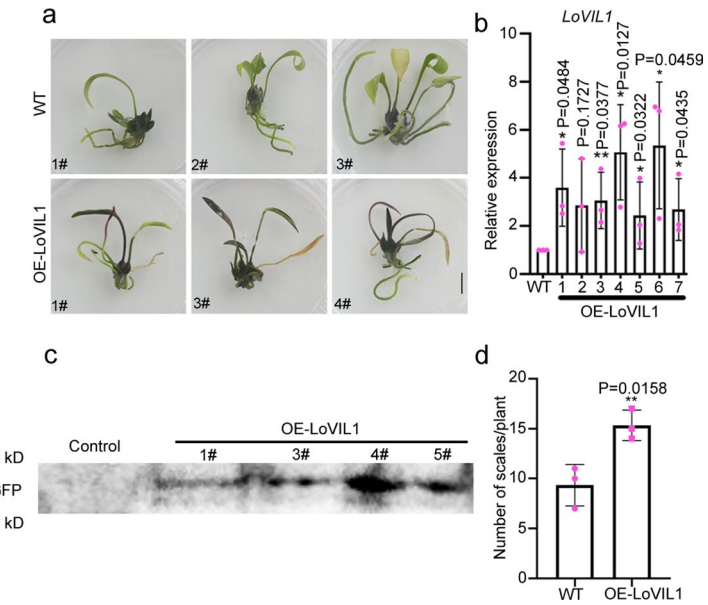
Extended Data Fig. 2 | Simulation of symplastic transport in central buds of dormant bulbs under different treatments by using CFDA. Deep dormant bulbs were cultivated on MS medium containing 1 mM N-Ethylmaleimide (NEM), 1 mM 2,3-Butanedione-monoxime (BDM), or 1 mM 2-Dioxy-D-glucose (DDG) for 4 weeks. MS medium was used as the control. Images showed the unloading of

CFDA in central buds after importing a 3-hour tracer import. In the control and NEM treatment, CFDA fluorescence was primarily confined to the vascular bundles (Vb) with weak signals. However, in the DDG and BDM treatments, the fluorescence was spread to the surrounding parenchyma cells. Consistent results were obtained in at least three independent bulbs at the same stage. Scale bar, 20 μ m.



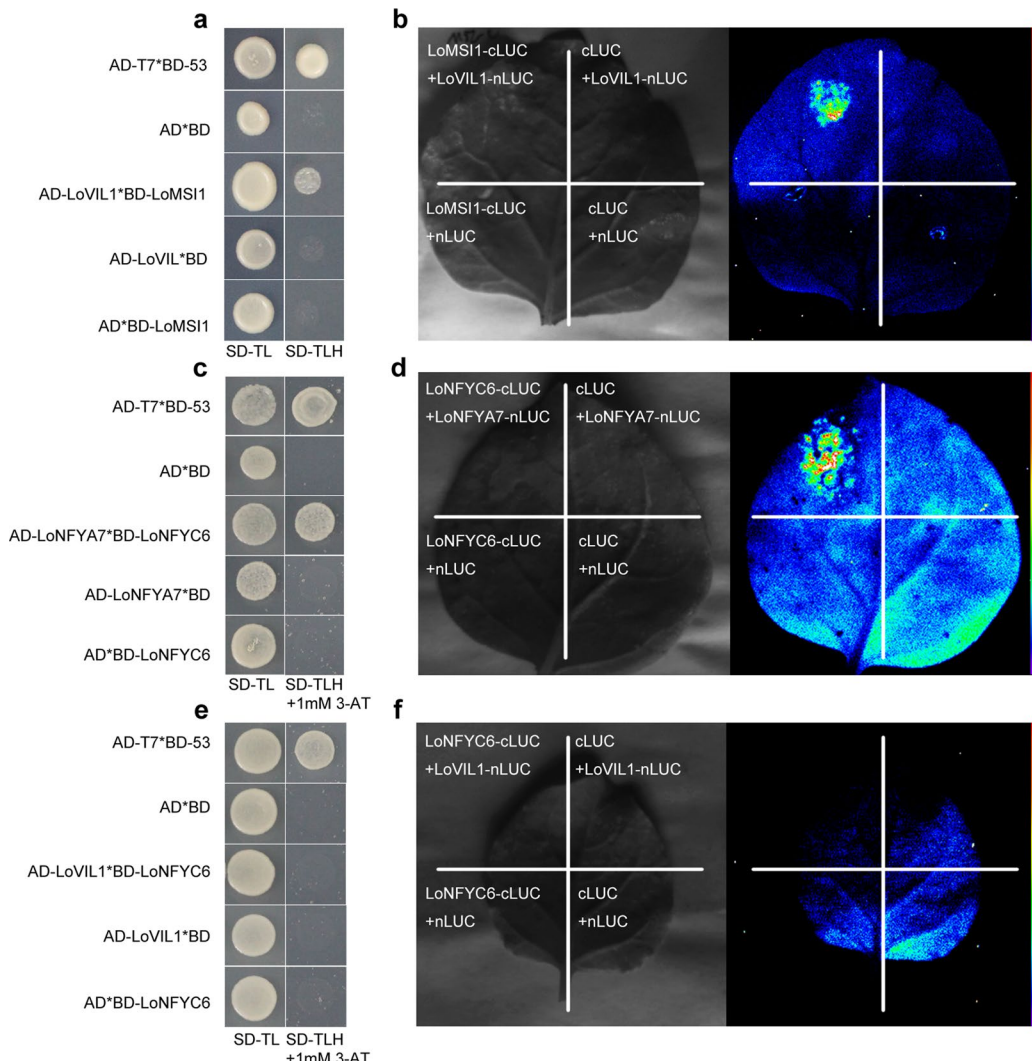
Extended Data Fig. 3 | Silencing of *LoVIL1* affects bulb growth transition and flower development. **a**, Phenotypes of TRV2-*LoVIL1* silenced plants after the sprouting stage (cold storage at 4 °C for 8 weeks and then 12 °C for 2 weeks). Scale bar, 1 cm. **b**, Detecting the expression of virus *COAT PROTEIN (CP)* in SAMs of TRV2-*LoVIL1* bulbs. *FP (F-BOX FAMILY PROTEIN)* served as the positive control. Noninfected plants were used as negative control (NC). **c**, Expression analysis of *LoVIL1* in TRV2-*LoVIL1* silenced plants using RT-qPCR. *FP (F-BOX FAMILY PROTEIN)* served as the internal reference gene. Data are presented as mean ± s.d. of three biological repeats (two-sided Student's *t*-test). **d,e**, Short plants (**d**) with

aborted or fewer flowers (**e**) were caused by silencing of *LoVIL1*. Images were captured 6 weeks after planting. Scale bars, 1 cm. **f-i**, Statistic analysis of flower number (**f**; n = 12 plants), flowering ratio (**g**; n = 12 plants), plant height (**h**; n = 14 plants), and leaf number (**i**; n = 10 plants) in *LoVIL1*-silenced plants 6 weeks after planting. TRV2 lines were used as controls. Data analysis in panels **c**, **f-i** employed a two-sided Student *t*-test. Data in panels **f**, **h** and **i** represent mean ± s.d. of the individual plants, while data in panel **g** are presented as mean ± s.d. of three biological replicates. M: DNA ladder marker.



Extended Data Fig. 4 | Overexpression of *LoVIL1* in lily. **a**, Transgenic lilies with OE-*LoVIL1* (*35S:eGFP-LoVIL1*) displayed accumulated anthocyanidin, early leaf senescence, and constant growth occurred. Scale bar, 1 cm. **b**, Expression of *LoVIL1* in OE-*LoVIL1* lilies using RT-qPCR. *FP* (*F-BOX FAMILY PROTEIN*) served as the internal reference gene. Data are presented as mean \pm s.d. of three biological

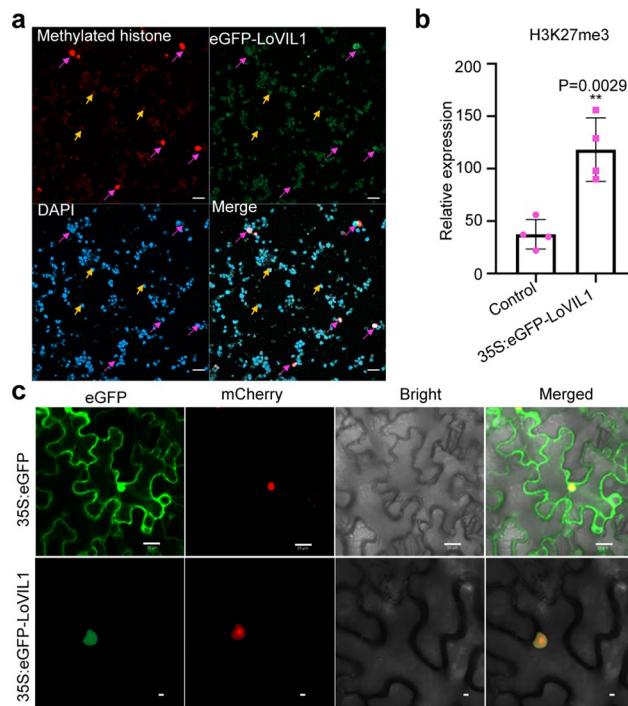
repeats (two-sided Student's *t*-test). **c**, Detecting GFP-fused proteins in OE-*LoVIL1* plants. GFP antibody was used for Western Blotting. Wildtype lily was used as the negative control. **d**, Quantification of scales number in OE-*LoVIL1* and wildtype (WT) plants after 3 months of culture. Data are presented as mean \pm s.d. of three independent plants (two-sided Student's *t*-test).


Extended Data Fig. 5 | LoVIL1 interacts with PRC2 complex but not LoNFYC6.

a, Validation of the interaction between LoVIL1 and PRC2 subunit LoMSI1 using yeast two-hybrid (Y2H) assay. AH109 yeast cells harbouring LoVIL1 and LoMSI1 were cultured on SD-TL (SD-Trp-Leu) and SD-TLH (SD-Trp-Leu-His) selecting media. Images were taken after 3 days of culture. At least five individual yeast colonies were tested for each construct, and one representative was shown. BD was used as the negative control; BD-53 was used as the positive control (same procedures in panels **c** and **e**). **b**, Split-luciferase complementation assay confirming the interaction between LoVIL1 and LoMSI1. The ORF of *LoVIL1* was cloned into the nLUC vector, and *LoMSI1* was cloned into the cLUC vector. cLUC is used as the negative control. Luciferase activities were determined

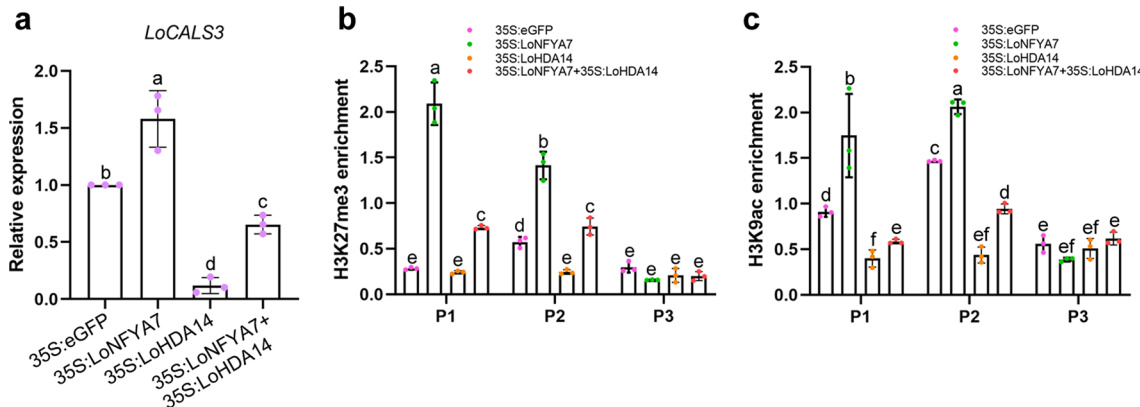
by luminescence imaging after 3 days of *N. benthamiana* leaf agroinfiltration. Color bars indicate luminescence intensity from weak (blue) to strong (red or white). Three biological replicates were performed with consistent results (same procedures in **d** and **f**). **c**, Validation of the interaction between LoNFYA7 and LoNFYC6 using Y2H assay. AH109 yeast cells harbouring LoNFYA7 and LoNFYC6 were cultured on SD-TL and SD-TLH + 1 mM 3-AT selecting media for 3 days.

d, Confirmation of the interaction between LoNFYA7 and LoNFYC6 using Split-luciferase complementation assay. **e**, LoVIL1 does not interact with LoNFYC6 in Y2H system. AH109 yeast cells harbouring LoNFYA7 and LoNFYC6 were cultured on SD-TL and SD-TLH + 1 mM 3-AT selecting media for 3 days. **f**, LoVIL1 does not interact with LoNFYC6 in the Split-luciferase complementation system.



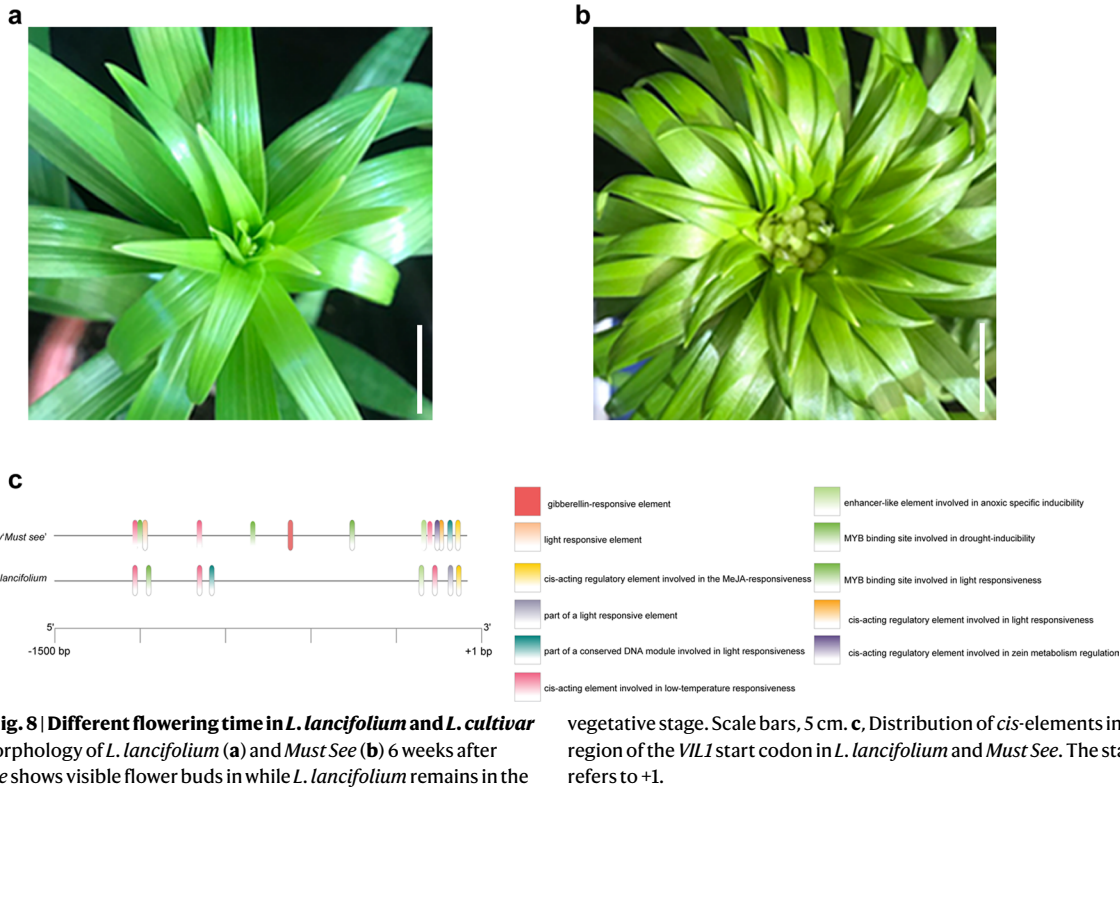
Extended Data Fig. 6 | Histone modification and subcellular localization of LoVIL1. **a,** *LoVIL1* enhances H3K27me3 modification. *Nicotiana benthamiana* leaves were transiently overexpressed with 35S:*eGFP-LoVIL1*. Samples were collected 3 days after agroinfiltration. Nuclei were collected and subjected to immunoprecipitation before confocal imaging. Blue, green, and red fluorescence represent the 4',6-diamidino-2-phenylindole (DAPI)-stained nuclei, eGFP-*LoVIL1* overexpressed nuclei, and methylated histone (H3K27me3), respectively. Non-transfected nuclei are indicated by yellow arrowheads while eGFP-*LoVIL1* overexpressed nuclei are indicated by purple arrowheads. Scale bars, 10 μ m. **b,** Quantification of methylation marks shown in panel **a**. The staining intensity of histone modification was compared by analyzing 10 pairs of transfected

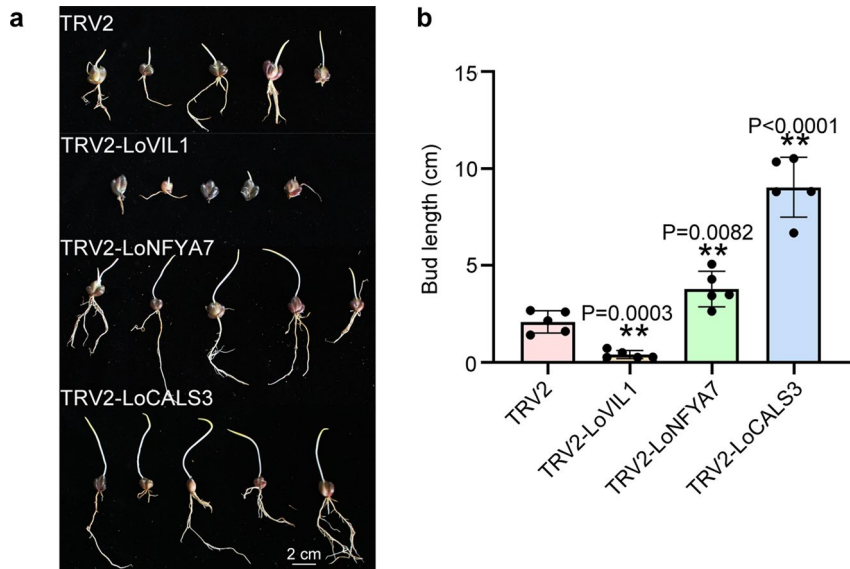
nuclei versus non-transfected nuclei in the same field of view. Four fields were analyzed using the ImageJ tool. Data are presented as mean \pm s.e. of four biological replicates (two-sided student's *t*-test). **c,** Subcellular localization of *LoVIL1* in *N. benthamiana* leaves. 35S:*eGFP-LoVIL1* was transiently overexpressed in *N. benthamiana* leaves. Images were captured after 3 days of agroinfiltration. mCherry fused Arabidopsis PLASTID RIBOSOMAL PROTEIN L24B (AtRPL24B; ATSG54600) was used as a nuclear marker. Fluorescence signals were collected using a fluorescence microscope with excitation wavelengths of 405 nm, 488 nm, and 561 nm. Scale bars, 20 μ m. Consistent results were obtained at least in three biological repeats.



Extended Data Fig. 7 | LoHDA14 antagonizes LoNFYA7 on *LoCALS3* expression through histone modification. **a**, Relative expression of *LoCALS3* in calluses transiently overexpressing *LoNFYA7*, *LoHDA14* or both (*LoNFYA7* and *LoHDA14*). **b**, Levels of H3K27me3 at *LoCALS3* locus in calluses transiently overexpressing *LoNFYA7*, *LoHDA14* or both (*LoNFYA7* and *LoHDA14*). **c**, H3K9ac levels at *LoCALS3*

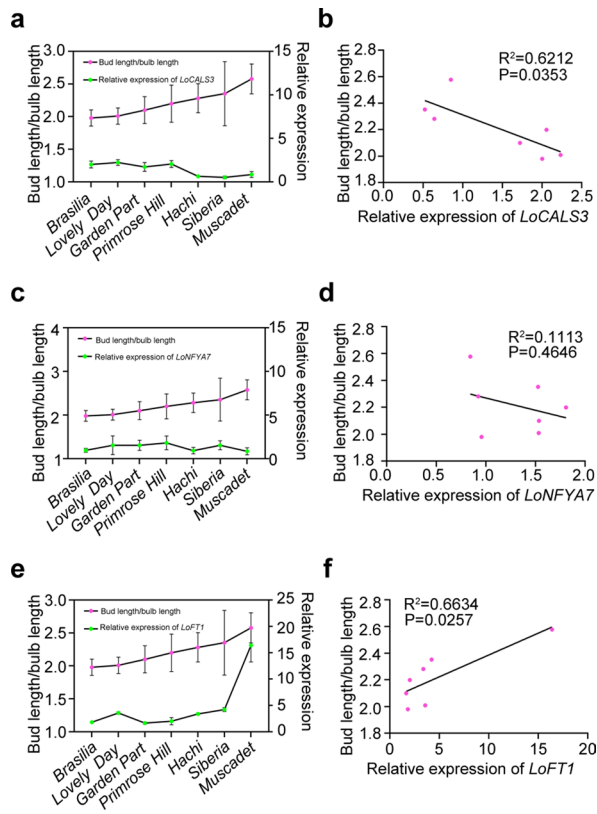
locus in calluses transiently overexpressing *LoNFYA7*, *LoHDA14* or both (*LoNFYA7* and *LoHDA14*). Three independent calluses were used and the data in panels **a-c** represent the mean \pm s.d. of three biological replicates. Different letters above bars in panels **a-c** indicate significant differences ($p = 0.001$) as determined by ANOVA Turkey's HSD tests for pairwise comparisons.





Extended Data Fig. 9 | Effects of *LoVIL1*, *LoNYA7*, and *LoCALS3* on bulbil growth transition in *L. lancifolium*. **a**, Phenotypes of *LoVIL1*-, *LoNYA7*-, and *LoCALS3*-silenced bulbils 14 weeks after infiltration. Deep-dormant *L. lancifolium* bulbils without cold storage were used. Scale bar, 2 cm. **b**, Measurement of

bud length in *LoVIL1*-, *LoNYA7*-, and *LoCALS3*-silenced bulbils 14 weeks after infiltration. Data are presented as mean \pm s.d. of five biological replicates ($n = 10$ bulbils per replicate; two-sided student *t*-test).



Extended Data Fig. 10 | Correlation between the dormancy trait and the expression levels of *LoCALS3*, *LoNFYA7*, and *LoFT1*. **a**, The development of central bud and the expression of *LoCALS3* in Oriental lilies 8 weeks of cold storage. **b**, Pearson correlation analysis of *LoCALS3* expression and central bud development. **c**, The development of central bud and the expression of *LoNFYA7* in Oriental lilies 8 weeks of cold storage. **d**, Pearson correlation analysis

of *LoNFYA7* expression and central bud development. **e**, The development of central bud and the expression of *LoFT1* in Oriental lilies 8 weeks of cold storage. **f**, Pearson correlation analysis of *LoFT1* expression and central bud development. Data in panels **a**, **c**, and **e** represent mean \pm s.d. of three biological replicates ($n = 30$ bulbs for bud development; $n = 3$ bulbs for the expression analyses).

Reporting Summary

Nature Portfolio wishes to improve the reproducibility of the work that we publish. This form provides structure for consistency and transparency in reporting. For further information on Nature Portfolio policies, see our [Editorial Policies](#) and the [Editorial Policy Checklist](#).

Statistics

For all statistical analyses, confirm that the following items are present in the figure legend, table legend, main text, or Methods section.

n/a Confirmed

- The exact sample size (n) for each experimental group/condition, given as a discrete number and unit of measurement
- A statement on whether measurements were taken from distinct samples or whether the same sample was measured repeatedly
- The statistical test(s) used AND whether they are one- or two-sided
Only common tests should be described solely by name; describe more complex techniques in the Methods section.
- A description of all covariates tested
- A description of any assumptions or corrections, such as tests of normality and adjustment for multiple comparisons
- A full description of the statistical parameters including central tendency (e.g. means) or other basic estimates (e.g. regression coefficient) AND variation (e.g. standard deviation) or associated estimates of uncertainty (e.g. confidence intervals)
- For null hypothesis testing, the test statistic (e.g. F , t , r) with confidence intervals, effect sizes, degrees of freedom and P value noted
Give P values as exact values whenever suitable.
- For Bayesian analysis, information on the choice of priors and Markov chain Monte Carlo settings
- For hierarchical and complex designs, identification of the appropriate level for tests and full reporting of outcomes
- Estimates of effect sizes (e.g. Cohen's d , Pearson's r), indicating how they were calculated

Our web collection on [statistics for biologists](#) contains articles on many of the points above.

Software and code

Policy information about [availability of computer code](#)

Data collection

RNA-Seq data was acquired by Illumina NextSeq sequencer;
Live luciferase images were collected by a CCD imaging machine (CHEMIPROHT 1300B/LND);
Relative activity of luciferase was measured by Glomax®-20/20 signal Tube Luminometer (Promega).
Microscopy images were collected by laser confocal fluorescence microscopy (ZEISS 880);
qRT-PCR data was collected by Step One PlusTM real-time PCR system (Applied Biosystems).

Data analysis

Statistical analyses were performed using one-way analysis of variance (ANOVA) followed by Tukey's HSD tests for pairwise comparisons;
GraphPad Prism 8.0.2 and DPS Statistics version 9.01 were used for analysis;
Graphs were generated by GraphPad Prism version 8.0.2;
Quantitation for callose intensity measured with ImageJ version 1.53c;
Gene Set Enrichment Analysis (GSEA) was conducted using the clusterProfiler package in R version 4.2.3 to determine whether genes belonging to a specific GO term show significantly concordant differences.

For manuscripts utilizing custom algorithms or software that are central to the research but not yet described in published literature, software must be made available to editors and reviewers. We strongly encourage code deposition in a community repository (e.g. GitHub). See the Nature Portfolio [guidelines for submitting code & software](#) for further information.

Data

Policy information about [availability of data](#)

All manuscripts must include a [data availability statement](#). This statement should provide the following information, where applicable:

- Accession codes, unique identifiers, or web links for publicly available datasets
- A description of any restrictions on data availability
- For clinical datasets or third party data, please ensure that the statement adheres to our [policy](#)

RNA-Seq data that support the findings of this study have been deposited in NCBI Bioproject database under the accession number PRJNA935924 (<http://www.ncbi.nlm.nih.gov/bioproject/935924>).

Sequence data of LoVIL1, LoNFYA7, LoCALS3, LoFT1, LoCAL55, LoCALS7, LoCALS10, LoCALS12 and LoHDA14 that support the findings of this study have been deposited in GenBank with the accession codes OQ469822, OQ469823, OQ469824, OQ469825, OQ469826, OQ469827, OQ469828, and OQ469829, LoHDA14 respectively.

Human research participants

Policy information about [studies involving human research participants and Sex and Gender in Research](#).

Reporting on sex and gender

N/A

Population characteristics

N/A

Recruitment

N/A

Ethics oversight

N/A

Note that full information on the approval of the study protocol must also be provided in the manuscript.

Field-specific reporting

Please select the one below that is the best fit for your research. If you are not sure, read the appropriate sections before making your selection.

Life sciences

Behavioural & social sciences

Ecological, evolutionary & environmental sciences

For a reference copy of the document with all sections, see nature.com/documents/nr-reporting-summary-flat.pdf

Life sciences study design

All studies must disclose on these points even when the disclosure is negative.

Sample size

Sample size was selected based on our prior knowledge and experience on the experimental variability of experiments and the desire to get statistically significant data to support meaningful conclusions. This resulted sample sizes were from n=3 to n=100 to ensure the variation was captured. Sample sizes were described in Figure legends or in the main text.

Data exclusions

No data was excluded.

Replication

Each experiment was repeated at least three times and similar results were obtained.

Randomization

For all studies, individual plants of different genotypes were randomized in the growth chambers to avoid environmental effects.

Blinding

Blinding is not common practice for this type of experiments.

Reporting for specific materials, systems and methods

We require information from authors about some types of materials, experimental systems and methods used in many studies. Here, indicate whether each material, system or method listed is relevant to your study. If you are not sure if a list item applies to your research, read the appropriate section before selecting a response.

Materials & experimental systems

n/a	Involved in the study
<input type="checkbox"/>	<input checked="" type="checkbox"/> Antibodies
<input checked="" type="checkbox"/>	<input type="checkbox"/> Eukaryotic cell lines
<input checked="" type="checkbox"/>	<input type="checkbox"/> Palaeontology and archaeology
<input checked="" type="checkbox"/>	<input type="checkbox"/> Animals and other organisms
<input checked="" type="checkbox"/>	<input type="checkbox"/> Clinical data
<input checked="" type="checkbox"/>	<input type="checkbox"/> Dual use research of concern

Methods

n/a	Involved in the study
<input checked="" type="checkbox"/>	<input type="checkbox"/> ChIP-seq
<input checked="" type="checkbox"/>	<input type="checkbox"/> Flow cytometry
<input checked="" type="checkbox"/>	<input type="checkbox"/> MRI-based neuroimaging

Antibodies

Antibodies used

Mouse monoclonal anti--GFP (Abmart GFP-Tag (7G9) Mouse mAb; catalog No. M20004S; clone: monoclonal; dilution 1:2000);
 Rabbit polyclonal anti--H3K27me3(Beyotime Biotechnology; catalog No. AF5710; clone: polyclonal; dilution 1:1000);
 Rabbit polyclonal anti--H3K9ac(Beyotime Biotechnology; catalog No. AF5611; clone: polyclonal; dilution 1:1000);
 Rabbit polyclonal anti--H3 (Proteintech; catalog No. 17168-1-AP; clone: polyclonal; dilution 1:1000);

Validation

Relevant information of antibodies used in this study is found here:
 Mouse monoclonal anti--GFP: <http://www.ab-mart.com.cn/page.aspx?node=%2059%20&id=%20971>
 Rabbit polyclonal anti--H3K27me3: <https://www.beyotime.com/product/AF5710.htm>
 Rabbit polyclonal anti--H3K9ac: <https://www.beyotime.com/product/AF5611.htm>
 Rabbit polyclonal anti--H3: <https://www.ptgcn.com/products/Histone-H3-Antibody-17168-1-AP.htm>